



Distinct Spatiotemporal Patterns of Atmospheric Total and Soluble Iron from Three Sources Revealed by Shipboard Online Observations in the Northwest Pacific

Tianle Zhang^{1,2}, Yaxin Xiang², Bingxing Zhu², Xiaohong Yao³, Xuehua Fan⁴, Yinan Wang⁴, Yuntao Wang⁵, Shuangling Chen⁵, Yan Zhang⁶, Fei Chai⁷, and Mei Zheng^{1,2}

Correspondence to: Mei Zheng (mzheng@pku.edu.cn)

15 Abstract

Non-dust emissions have been increasingly recognized as important contributors to atmospheric iron (Fe), influencing marine productivity through enhanced bioavailable Fe inputs. However, accurately quantifying the contributions and spatiotemporal variability of non-dust sources remains challenging due to relatively low time-resolution of traditional filterbased analytical methods. In this study, the contributions of non-dust emissions to atmospheric total and soluble Fe in the Northwest Pacific were quantified based on online measurements from three ship-based observation campaigns in 2021– 2022. A Positive Matrix Factorization (PMF) model was applied for source apportionment. Results showed non-dust emissions contributed substantially to atmospheric Fe, accounting for 21%-48% of total Fe across different regions and seasons. Importantly, their contributions to soluble Fe were significantly higher, reaching 79%–98% and largely dominating the bioavailable Fe supply in the study area. Among non-dust sources, land anthropogenic emissions contributed significant portion of both total and soluble Fe, whereas ship emissions contributed small portion to total Fe but was major source of soluble Fe, particularly in coastal regions. In summer, ship emissions over coastal waters even exceeded land anthropogenic sources, becoming the dominant contributor to soluble Fe. Additionally, Fe from non-dust sources exhibited stronger spatial variability than dust source. The concentrations of land anthropogenic Fe differed by 3-5 times between coastal and openocean areas during the same cruises, while ship-derived Fe varied by an order of magnitude or more. This study offers critical observational evidence to advance understanding of how diverse emission sources shape atmospheric composition in Asian continental outflow regions.

¹Institution of Ocean Research, Peking University, Beijing 100871, China

²State Key Laboratory of Regional Environment and Sustainability, College of Environmental Sciences and Engineering, and Center for Environment and Health, Peking University, Beijing 100871, China

³Ocean University of China, Qingdao 266100, China

⁴ Institute of Atmospheric Physics, Chinese Academy of Sciences, Beijing 100029, China

⁵Second Institute of Oceanography, Ministry of Natural Resources, Hangzhou 310012, China

⁶Department of Environmental Science and Engineering, Fudan University, Shanghai 200438, China

⁷College of Ocean and Earth Sciences, Xiamen University, Xiamen 361005, China





1 Introduction

35

40

45

50

55

Iron (Fe) in marine aerosols have been extensively studied over the past few decades due to its critical role in marine primary productivity enhancement and global climate regulation through the marine biological pump (Martin, 1990; Jickells et al., 2005; Myriokefalitakis et al., 2018; König et al., 2022). Over geological timescales, atmospheric Fe has been considered to originate mainly from dust emissions (Lambert et al., 2015). Since the industrial revolution, however, the intensity of Fe emissions from anthropogenic activities such as coal combustion, oil combustion, and industrial processes has increased significantly (Krishnamurthy et al., 2009). These sources have become important contributors to the global atmospheric Fe budget, especially in densely populated and fast-developing regions such as East Asia (Zhu et al., 2022; Chen et al., 2024) and its downwind Northwest Pacific Ocean (Zhang et al., 2024; Bunnell et al., 2025).

Iron from non-dust emissions generally exhibits higher solubility than that from mineral dust (Fu et al., 2012; Oakes et al., 2012). This made non-dust emissions especially important for atmospheric soluble Fe, which is the bioavailable form that marine phytoplankton could more readily utilize (Gledhill and Buck, 2012; Tagliabue et al., 2017). Therefore, understanding the quantitative contributions and spatiotemporal variations of Fe from non-dust sources is essential for characterizing the supply of soluble Fe to the ocean and for evaluating the impacts of human activities on marine ecosystems and climate through Fe cycling.

Currently, quantitative estimates of Fe sources in the marine atmosphere rely primarily on numerical models (Myriokefalitakis et al., 2018; Ito et al., 2019). A variety of models such as the Integrated Massively Parallel Atmospheric Chemical Transport (IMPACT) (Ito, 2015; Ito et al., 2019), the Community Atmospheric Model (CAM) (Matsui et al., 2018; Scanza et al., 2018), the Goddard Earth Observing System-Chemical transport (GEOS-Chem) (Alexander et al., 2009; Johnson and Meskhidze, 2013), and the Community Multiscale Air Quality (CMAQ) (Lin et al., 2015; Jiang et al., 2024) have been applied to simulate atmospheric Fe concentrations and sources. Based on model simulation, it was found that non-dust sources play an important role in shaping the spatial and temporal distributions of atmospheric soluble Fe concentrations and deposition over the global ocean (Wang et al., 2015; Ito et al., 2019; Hamilton et al., 2020). Specifically, anthropogenic emissions from East Asia substantially contributed to soluble Fe over the North Pacific (Wang et al., 2015; Hamilton et al., 2020; Ito and Miyakawa, 2023), while wildfires were identified as a major soluble Fe source in the Southern Ocean (Matsui et al., 2018; Hamilton et al., 2020; Liu et al., 2022b).

In contrast to the rapid development of numerical models, direct observations of atmospheric Fe over the ocean remain scarce, particularly those providing quantitative evidence for source apportionment (Zhang and Zheng, 2024). Field measurements can provide valuable constraints and complementary insights to models by offering a more detailed understanding of Fe sources over oceanic regions. For example, studies by Kurisu et al. (2021) and Pinedo-Gonzalez et al. (2020), using ship-based sampling and Fe isotope analysis, confirmed the significant contribution of anthropogenic emissions from East Asia to soluble Fe in marine atmosphere and even in surface seawater in the downwind Pacific Ocean. Additionally, Conway et al. (2019) reported that even in



65

75

80

90



the dusty North Atlantic Ocean, when influenced by continental air masses from Europe, non-dust sources could account for 50%–100% of the atmospheric soluble Fe.

To date, ship-based aerosols observations have primarily relied on traditional filter-based sampling methods. These required long sampling durations and thus limited both the temporal resolution and the volume of data collected (Kurisu et al., 2021; Ge et al., 2024). To address this limitation, our previous work developed a shipborne online measurement approach for atmospheric Fe, which improved the temporal resolution of observations from daily to hourly scales. By integrating these continuous measurements with a source apportionment receptor model, we were able to quantitatively resolve contributions from multiple Fe sources in the marine atmosphere (Zhang et al., 2024). This approach proved highly effective in generating large, source-resolved datasets in marine environments. Nevertheless, observational datasets covering different seasons and oceanic regions remain limited, hindering comprehensive assessments of non-dust Fe variability and its climatic implications.

In this study, we present an analysis of atmospheric Fe based on online measurement data collected during three research cruises across the Chinese marginal seas and the open Northwest Pacific between 2021 and 2022. Combing source apportionment receptor model and empirical Fe solubility parameters, the contributions of non-dust emissions to both total and soluble atmospheric Fe was evaluated. We further examine the spatial and seasonal variability of these sources and distinguish the relative contributions from land-based anthropogenic emissions and ship exhaust. These findings provide new observational constraints on the magnitude and distribution of total and soluble Fe from non-dust emissions, offering important insights into their role in regulating marine biogeochemistry in a major continental outflow region.

2 Methodology

2.1 Cruise information

This study incorporated data collected during three research cruises (BY, NWP1, and NWP2) conducted between May 2021 and July 2022. The cruise tracks are shown in Fig. 1a. The BY cruise was carried out in the Chinese marginal seas, primarily in the Bohai Sea and Yellow Sea, aboard the R/V *Lanhai 101* from April 14 to 27, 2022 (green line in Fig. 1a). The NWP1 and NWP2 cruises covered the Yellow Sea, East China Sea, and areas south and east of Japan in the open Northwest Pacific. NWP1 was conducted aboard the R/V *Dongfanghong 3* from May 10 to June 17, 2021 (blue line in Fig. 1a). During the NWP2 cruise, instrument malfunctions occurred. Therefore, this study focuses only on the cruise segment with normal instrument performance, indicated by the red line in Fig. 1a. This segment was conducted from June 18 to July 6, 2022, also aboard the R/V *Dongfanghong 3*.



100

105

110



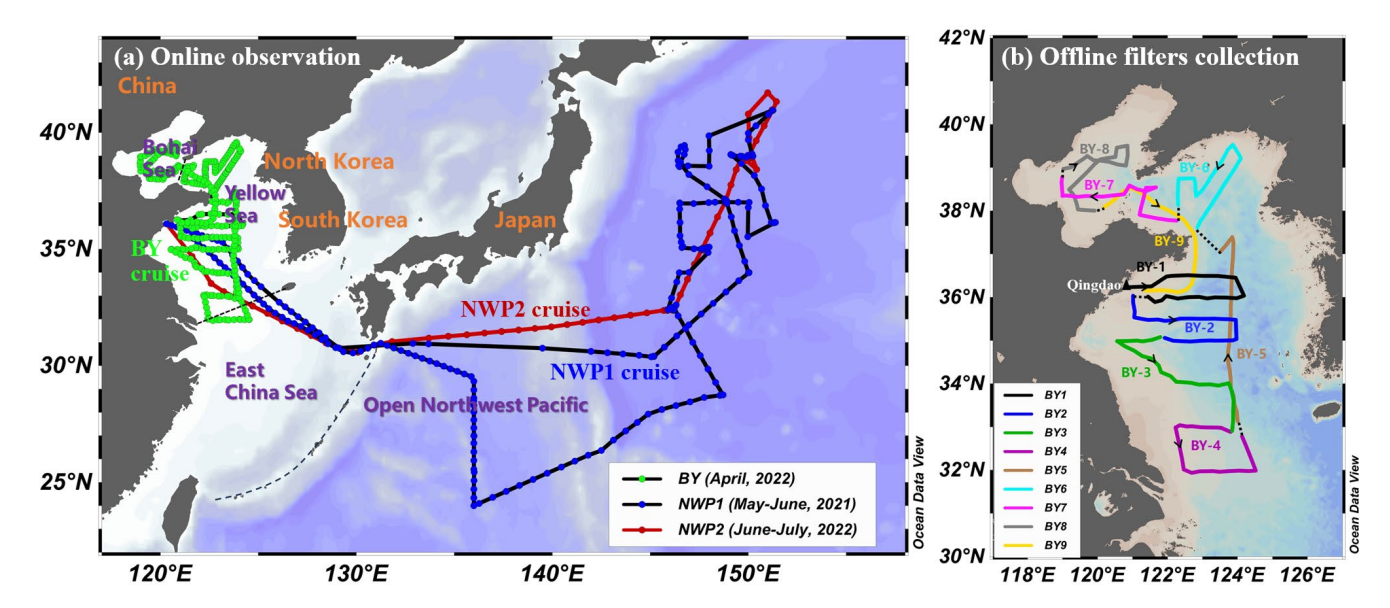


Figure 1. Cruise tracks in the Chinese marginal seas and the open Northwest Pacific during 2021–2022. (a) Shipborne online observation; each dot represents an online sample. (b) Filter samples collection; each solid line represents an offline filter sample. BY refers to the cruise conducted in 2022 over the Bohai and Yellow Seas; NWP1 and NWP2 refer to cruises conducted in 2021 and 2022, respectively, in the Northwest Pacific.

2.2 Shipborne online observations

During the three cruises, an online multi-element analyzer (Xact 625) was used to continuously measure elemental concentrations in atmospheric aerosols. The Xact 625 (Cooper Environmental Services LLC) is designed to monitor aerosols elemental composition at high time resolution (Yanca et al., 2006) and has been certified by the U.S. Environmental Protection Agency (EPA) for ambient air monitoring (https://archive.epa.gov/nrmrl/archive-etv/web/pdf/p100fk6b.pdf). The instrument operates at an air sampling flow rate of 16.7 L min⁻¹. Ambient aerosols pass through a size-selective inlet and then flow through the instrument tubing before being deposited onto a reel-to-reel polytetrafluoroethylene (PTFE) filter tape. The sampling duration (time resolution) of each sample is adjustable between 0.5 and 4 hours. After each sampling cycle, the reel advances to move the filter tape segment with the sample spot to the analysis position. Elemental masses of various target elements at the sample spot are automatically determined using a built-in X-ray fluorescence (XRF) system. The instrument calculates ambient mass concentrations of each element based on the sampling duration and flow rate. The Xact 625 used in this study is capable of simultaneously analyzing 22 elements, including K, Fe, Ca, Zn, Mn, Ba, Cu, Pb, V, Ni, As, Se, Ag, Cd, Cr, Hg, Co, Sn, Sb, Ga, Au, and Tl.

During the BY cruise, the Xact 625 was installed in a laboratory on the main deck (Fig. S1a), with the sampling inlet secured to the portside railing of the boat deck, approximately 10 meters above sea level. During the NWP1 and NWP2 cruises, the instrument was installed inside a container on the foredeck (Fig. S1b), with the sampling inlet fixed to the



115

120

125

130

135

140



container roof, approximately 12 meters above sea level. As shown in Fig. S1, the inlets were positioned forward of the ship's funnel and at a lower height, minimizing the influence of the ship's exhaust plume, which typically dispersed aft and upward.

For particle size selection, the Xact 625 was equipped with a PM_{2.5} inlet during the NWP1 cruise, which selectively sampled fine particles with aerodynamic diameters less than or equal to 2.5 μm. In contrast, a PM₁₀ inlet was used during the BY and NWP2 cruises to extend the measurements to coarse particles with aerodynamic diameters less than or equal to 10 μm. This size range is also comparable to those covered in several aerosol models, such as CAM (0.1–10 μm), CMAQ (0.1–10 μm), GEOS-Chem (0.1–12 μm), and IMPACT (<1.26–20 μm) (Binkowski and Roselle, 2003; Myriokefalitakis et al., 2018).

The temporal resolution of the measurements was also adjusted according to ambient conditions. During the BY cruise, where elemental concentrations were relatively high and the cruise track was short, the resolution of Xact 625 was set to 1 h and further refined to 0.5 h in parts of the northern Yellow Sea to maximize data collection. In contrast, during the NWP1 cruise, the resolution was set to 2 h in marginal seas and 4 h over the open Northwest Pacific. In the summer NWP2 cruise, when elemental concentrations were lower, the resolution was set to 4 h, which ensured the lowest detection limits.

2.3 Filters collection and laboratory analysis

In addition to shipborne online observations, filter samples were collected during the BY cruise using a TH-16A sampler (Wuhan Tianhong Environmental Protection Industry Co., Ltd.). The TH-16A features four sampling channels, each operating at a constant flow rate of 16.7 L min⁻¹. PTFE filters (46.2 mm diameter, Whatman) were used to collect atmospheric particulate matter. As shown in Fig. S1a, the sampler was installed on the compass deck, located away from the ship's funnel to reduce potential contamination. Sampling was carried out only during vessel navigation and was paused while the ship was anchored. Each filter sample represented a cumulative 24-hour sampling period. In total, nine PM₁₀ filter samples were collected during the BY cruise (see BY1–BY9 in Fig. 1b).

Both total and soluble elements in the filters were analyzed. Detailed procedures are provided in the Supplementary Material (Text S1). Briefly, total elements were extracted by microwave-assisted acid digestion using a mixture of nitric acid (HNO₃), hydrogen peroxide (H₂O₂), and hydrofluoric acid (HF) (Zhang et al., 2022). After digestion, the solution was heated to near dryness and reconstituted with 20 mL of 1% (v/v) HNO₃, followed by filtration through a 0.22 µm polyethersulfone (PES) syringe filter. Soluble elements were extracted by horizontally shaking the filter fragments for 2 hours in an ammonium acetate–acetic acid buffer (pH 4.7) at room temperature. Compared to deionized water, this buffer better simulates Fe dissolution in ligand-added leaching conditions (Perron et al., 2020). The resulting solution were filtered through a 0.22 µm PES syringe filter and acidified to 1% (v/v) HNO₃. Both total and soluble elemental extracts were analyzed using inductively coupled plasma mass spectrometry (ICP-MS; iCAP Q, Thermo Fisher Scientific) for the concentrations of Al, Fe, Ba, Mn, Cr, Cu, Zn, Pb, V, Ni, As, Se, Cd, and Sb.



155

160

165

170

175



145 **2.4 Data quality control**

2.4.1 Data quality control of Xact 625 online measurement

The data quality control procedures for the Xact 625 measurements are described in detail in our previous study (Zhang et al., 2024). In summary, the quality control process involved three key steps: (1) calibration of the Xact 625 instrument using elemental standards with certified concentrations, followed by verification of instrumental stability through manual review of automated quality control (QC) logs; (2) evaluation of the proportion of samples with elemental concentrations above the minimum detection limits (MDL) for 22 elements, alongside the identification and removal of outliers; and (3) exclusion of samples potentially influenced by ship exhaust, based on apparent wind direction and apparent wind speed criteria.

The quality control results from Step 1 indicated stable operation of the Xact 625 instrument during the BY and NWP1 cruises. However, a mid-cruise instrument malfunction occurred during the NWP2 cruise. As shown in Fig. S2, both the QA-Pd values (used to monitor XRF fluorescence intensity) and the stability of the built-in Cr, Pb, and Cd reference rods, which were automatically measured through daily QC protocols, deviated significantly after July 6, 2022. These deviations indicate that the instrument was no longer operating under normal conditions, resulting in unreliable measurements. Therefore, for the NWP2 cruise, only data collected between June 18 and July 6 were discussed in this study. In addition, blank tests were conducted on the PTFE filter rolls used in the Xact 625 during each cruise. The results showed abnormally high blank values for K in both the BY and NWP2 cruises. As a result, K data from these two cruises were excluded from further discussion in this study.

The quality control (QC) results from Step 2 showed that the concentrations of the target element (Fe) in all samples from the three cruises were above the MDL. Elements other than Fe were mainly used as input variables in the Positive Matrix Factorization (PMF) receptor model to assist in source identification of Fe. According to Huang et al. (1999), chemical species used as input data for the PMF model should have more than 80% of their values above the MDL. Therefore, twelve elements that met this criterion were initially selected. These included K (only for the NWP1 cruise), Ca, Mn, Fe, Ni, Cu, Zn, Se, Au, Cd, Ba, and Pb. Among these elements, Au was excluded due to the lack of understanding of its emission sources. Cd was further excluded due to low confidence in its concentration measurements, as its concentrations were significantly higher than those reported in previous studies (Table S1). Instead, the specific tracers of ship emission (V) (Zhao et al., 2013) and coal combustion (As) (Tian et al., 2015) were additionally selected, although they only have 75% and 39% values above detection limits. Based on the time series of these elemental concentrations, five outliers were identified. These included two for Ca, two for Ba, and one for Zn. The outliers were replaced with the average concentrations of the corresponding elements in the samples immediately before and after the outliers. Details on the definition and screening method of outliers were provided in Supplementary Text S2.

In Step 3, samples potentially contaminated by ship exhaust from the research vessel were identified through a two-step procedure. First, 8 samples with an average apparent wind speed (vector sum of real wind and ship wind) below 2 m s⁻¹ were



180

185

190

195

200

205



excluded (Gao et al., 2013; Zhang et al., 2024). Second, 75 samples were selected only if, during the respective sampling cycle, the inlet was downwind of the ship's funnel and the apparent wind speed maintained a minimum of 2 m s⁻¹ for at least 5 minutes. Using V and Ni as tracers for ship smoke (Zhao et al., 2013), it was found that 14 of the 75 selected samples exhibited concentrations of V and Ni that exceeded the cruise-averaged values. These 14 samples were considered potentially contaminated by ship smoke and were excluded from further analysis. As a result, a total of 644 valid samples remained out of the original 666 samples.

2.4.2 Data quality control of filter chemical analysis

For elemental analysis of the filter samples in the laboratory, two certified standard reference materials of Luochuan loess from Shaanxi, China (GBW07454 (GSS-25), certified Fe content: $3.01 \pm 0.05\%$) were digested alongside the ambient aerosol samples. Based on the specific aliquots used, the certified total Fe contents of the two reference materials were 189.44–195.84 µg and 180.56–186.66 µg, respectively. The Fe concentrations measured by ICP-MS were 192.26 µg and 182.32 µg, respectively, both of which fell within the certified ranges, thereby confirming the accuracy of the analytical procedure. In addition, internal standard elements (Sc, Ge, Y, and In) were spiked into the test solutions during ICP-MS analysis. The recovery rates of these internal standards were consistently maintained within the range of 80%–120% across all samples, further validating the reliability of the analysis.

Four field blanks were analyzed, including two blanks for acid digestion and two for buffer extraction. Elemental concentrations in ambient samples were corrected by subtracting the corresponding blank values. For the elements discussed in this study (Al, Pb, V, Fe, and soluble Fe), concentrations in the blank samples contributed relatively little to those in ambient samples. Specifically, the average concentrations of Al, Pb, V, Fe, and soluble Fe in blank samples accounted for 1.7%, 4.0%, 7.2%, 13.4%, and 0.29% of their respective concentrations in ambient samples.

2.5 Source apportionment receptor model

The Positive Matrix Factorization receptor model was applied using the U.S. EPA PMF version 5.0 software to apportion the sources of Fe in marine aerosols. As a multivariate factor analysis tool, the PMF model does not require the input of source profiles, but relies on chemical tracers to identify emission sources (Paatero and Tapper, 1994; Gary et al., 2014). The PMF model requires two key inputs: a measured species concentration matrix (X) and their associated uncertainty values, which are used to weight individual data points. The methodology for calculating uncertainties is provided in Supplementary Text S3. As shown in Equations (1) and (2), PMF decomposes the species concentration matrix (X) into a factor contribution matrix (G) and a factor profile matrix (F) by minimizing the objective function Q using a weighted least squares approach. Source identification is carried out by interpreting the chemical tracer signatures in the factor profiles (matrix F) and the factor contributions (matrix G) is used to quantitatively apportion contributions of each source.



215

220

225

230

235



$$X = GF + E \tag{1}$$

210
$$Q(E) = \sum_{i=1}^{n} \sum_{j=1}^{m} \left[\frac{e_{ij}}{u_{ij}} \right]^{2}$$
 (2)

where matrix X (species concentrations) has dimensions $n \times m$, where n is the number of samples and m is the number of chemical species; matrix G (factor contributions) has dimensions $n \times p$, where p represents the number of factors (emission source types); matrix F (factor profiles) has dimensions $p \times m$, describing the chemical composition of each factor; matrix E (residual matrix) also has dimensions $n \times m$ and represents the difference between the measured concentrations (X) and the model-reconstructed values (GF); e_{ij} and u_{ij} in equation (2) are the residuals and uncertainties of the species j in sample i, respectively.

The PMF has been successfully applied to investigate Fe sources in urban aerosols (Zhu et al., 2022; Meng et al., 2023; Chen et al., 2024). However, PMF requires a relatively large sample size, typically at least five times the number of input chemical species, therefore generally requiring 50 samples or more (Cao, 2014). This requirement has consequently constrained its application in ship-based studies, where the number of offline filter samples is often insufficient. Therefore, the application of PMF in marine aerosols studies has primarily relied on the integration of multi-cruise offline datasets (Wang et al., 2013), long-term observations at fixed island stations (Li et al., 2023), or shipborne online measurements (Zhang et al., 2024).

3 Results and discussions

3.1 Sources of total Fe in marine aerosols

3.1.1 Source apportionment of total Fe by PMF

As described in the Methodology section, quality-controlled datasets were incorporated into the PMF analysis. Specifically, 229 online PM_{2.5} samples containing 12 elements from the NWP1 cruise, 97 online PM₁₀ samples containing 11 elements from the NWP2 cruise, and 318 online PM₁₀ samples containing 11 elements from the BY cruise were used. The NWP1 cruise uniquely included K in its elemental dataset, which was absent in the other two campaigns. In addition, NWP1 targeted PM_{2.5} fraction measurements, whose source profiles may differ from those of PM₁₀ particles (Zhang et al., 2014b). For these reasons, the NWP2 and BY cruise datasets were processed together in the PMF model, whereas the NWP1 cruise data were processed separately. The optimal number of PMF factors was determined based on mathematical diagnostic indicators from the PMF Guide and on the variations of chemical tracers in each factor. Further details are provided in Text S4 in the supplementary materials. In brief, the results indicated that three factors provided the best fit. The corresponding factor profiles are presented in Fig. 2.

As depicted in Fig. 2a, the three-factor profiles derived from marine atmospheric PM_{10} samples in this study exhibited three clearly distinct emission sources. Factor 1 showed a significant contribution (>50%) to elements Ca, Fe, and Ba,



245

250

255

indicating a clear dust source signature (Zhang et al., 2014b; Bi et al., 2019; Zhang et al., 2023b). Factor 2 demonstrated substantial contributions to multiple elements, including Mn, Cu, Zn, Pb, As, and Se, representing emissions from land anthropogenic activities, such as industrial processes and coal combustion (Tian et al., 2015; Liu et al., 2018). Factor 3 was characterized by high contributions to V and Ni, established tracers of heavy oil combustion, indicating its origin from ship emissions (Zhao et al., 2013; Yu et al., 2021). The three-factor profiles for PM_{2.5} samples, presented in Fig. 2b, were similar to those of PM₁₀, with only minor differences in the concentrations and contribution percentages of certain elements within the factors. These PM_{2.5} factor profiles also represented the same three source categories, namely dust, land anthropogenic, and shipping sources.

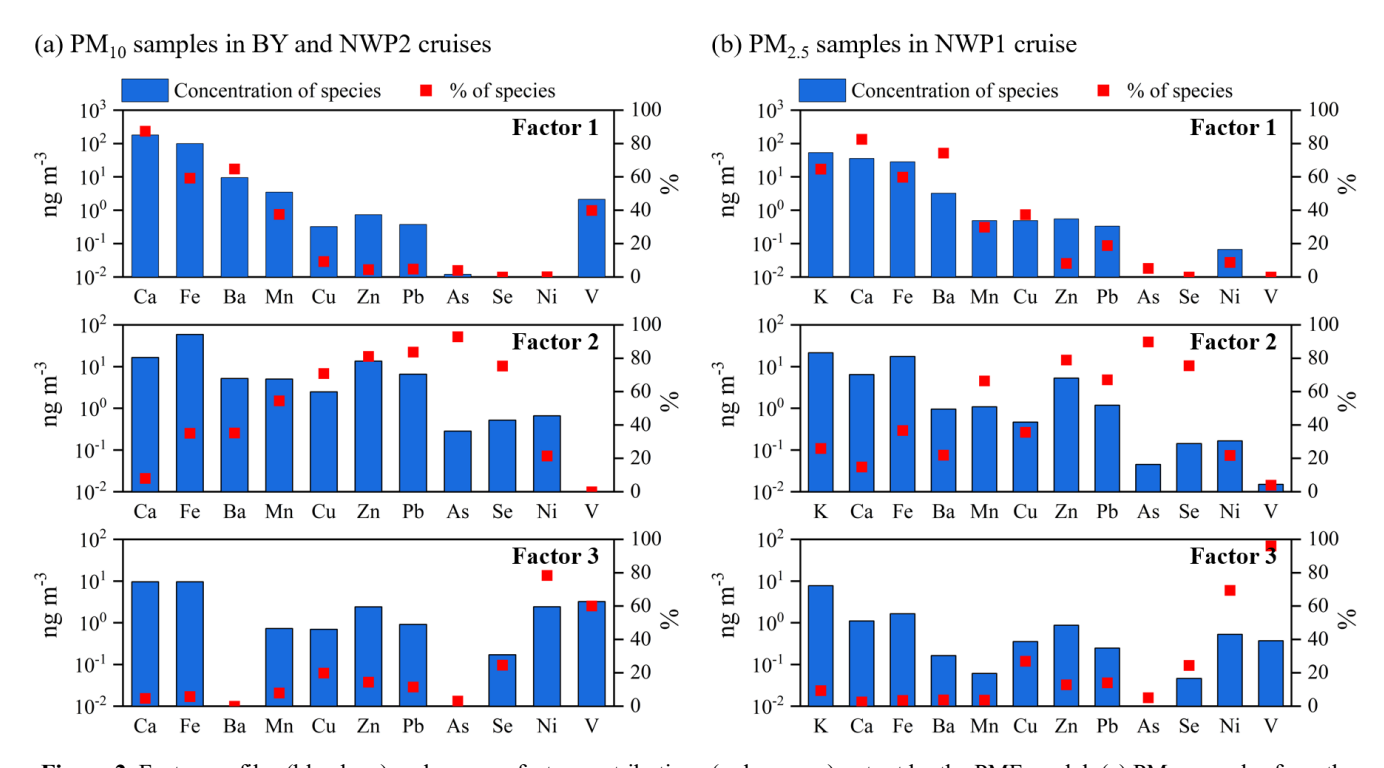


Figure 2. Factor profiles (blue bars) and average factor contributions (red squares) output by the PMF model. (a) PM₁₀ samples from the BY and NWP2 cruises. (b) PM_{2.5} samples from the NWP1 cruise.

3.1.2 Comparison of filter-based chemical tracers with PMF results derived from online measurements

Previous traditional filter-based studies often had small sample sizes, which limited the use of receptor models in earlier work. Researchers therefore relied on chemical tracers for qualitative source identification of marine aerosols. Common choices included Al as a dust tracer, Pb as an indicator of land-based anthropogenic pollution, and V as an indicator of ship emissions from heavy oil combustion (Hsu et al., 2010; Guo et al., 2014; Lee et al., 2017). In this study, we compared PMF-



265

270

275



resolved Fe from the Xact 625 online measurements with these filter-based tracers during the BY cruise to evaluate how well these tracers captured source-specific Fe concentrations. The filter samples were aligned in sampling time with the online observations, and the PMF-resolved Fe concentrations were plotted against the concentrations of Al, Pb, and V measured on the filters (Fig. 3).

As shown in Figs. 3a and 3b, Al and Pb demonstrated strong capability as tracers for dust-derived Fe and land anthropogenic Fe, respectively. The corresponding linear regression analyses yielded R^2 of 0.99 and 0.83, respectively. In contrast, the R^2 for the linear regression between V and ship-derived Fe concentration was lower, at 0.68 (Fig. 3c). Inspection of the scatter plot for ship-derived Fe versus V identified an outlier (circled with a dashed line) positioned below the regression line, indicating a higher V concentration relative to its ship-derived Fe level. This suggests that an additional source contributed V to this sample. This sample (BY9, Fig. 1b) was collected during an intense dust event transported from East Asia (see Section 3.1.3). Filter analysis showed an Al concentration of 3011 ng m⁻³, indicating substantial dust influence. The Al/V ratio for this sample was 420, close to the crustal ratio of 691 (Li and Yuan, 2011) and much higher than the average ratio in other samples (31.9 \pm 31.9). These results suggest that intense dust events elevated V concentrations in this sample.

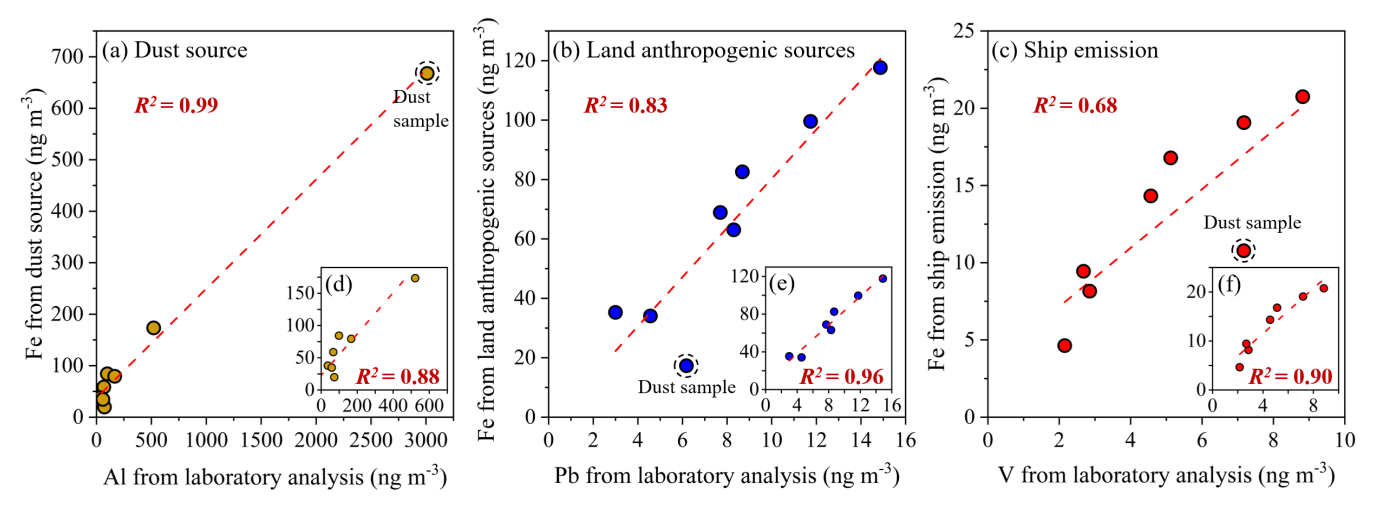


Figure 3. Comparing PMF results from Xact 625 online measurements with chemical tracers from offline filter analyses. (a) Fe concentration from dust source versus Al concentration. (b) Fe concentration from land anthropogenic sources versus Pb concentration. (c) Fe concentration from ship emission versus V concentration. (d)-(f) same as (a)-(c), but excluding the dust sample data point. The dashed circle represents the dust sample, and the red dashed lines represent the linear regression lines for these scatter plots.

When the dust-affected sample was excluded, the R² for ship-derived Fe versus V increased markedly from 0.68 to 0.90 (Figs. 3c and 3f), while the R² for land anthropogenic Fe versus Pb improved from 0.83 to 0.96 (Figs. 3b and 3e). Conversely, the R² for dust-derived Fe versus Al decreased slightly from 0.99 to 0.88 (Figs. 3a and 3d). This pattern reinforces that dust events strengthen the applicability of Al as a dust tracer but reduce the reliability of non-dust tracers, particularly V for ship



285

295

300

305



emissions. Using V to trace ship-derived particles during periods or in regions with high dust influence may therefore lead to overestimation.

These findings illustrate the limitations of directly using filter-based chemical tracers for source-specific Fe (or other species). Receptor models such as PMF are preferable, as they provide quantitative source apportionment that accounts for tracer overlap among sources. While PMF still uses tracers to identify source categories, its results typically indicate that the traced source is the primary, but not the sole, contributor to the tracer. For example, in Fig. 2a, V had the highest loading in the ship emission factor (factor 3) but also appeared in the dust factor (factor 1) due to dust event interference. Such source apportionment better captures the complexity of the real-world atmospheric environment. Moreover, because PMF is driven by observational data, it generally yields more reliable results than purely numerical models.

3.1.3 Sources of atmospheric total Fe in Chinese marginal seas

The Bohai Sea and Yellow Sea lie adjacent to mainland China, roughly between 30°N and 40°N. Under the prevailing westerlies, dust emissions from northern China and Mongolia can be transported to these regions (Zhang et al., 2023b; Ji et al., 2024). Owing to their proximity to the North China Plain, the Bohai Sea and Yellow Seas are also strongly influenced by anthropogenic pollutants (Liu et al., 2022a; Xu et al., 2023), resulting in complex aerosols sources.

Ship-based online measurements of atmospheric Fe conducted in April 2022 (Fig. 4a) showed Fe concentrations in PM₁₀ samples ranging from 25.34 to 2874 ng m⁻³, with a median value of 133.2 ng m⁻³. Along the cruise track, the mean Fe concentration was 130.9 ± 74.64 ng m⁻³ in the Bohai Sea and 247.6 ± 302.5 ng m⁻³ in the Yellow Sea. Overall, these values were comparable to recent shipborne observations in nearby sea areas. For example, Yang et al. (2020) reported an Fe concentration of 543.1 ng m⁻³ in atmospheric TSP (total suspended particulates) over the Yellow Sea–East China Sea region in spring 2017, and Ge et al. (2024) reported a value of 258 ng m⁻³ of Fe in atmospheric TSP over the East China Sea in autumn 2021.

However, compared with much earlier measurements, the Fe concentrations observed during this cruise were lower. For instance, Zhang et al. (2014a) reported a mean Fe concentration of 728.2 ng m⁻³ in PM_{2.5} over Tuoji Island in the Bohai Sea in spring 2012, and Wang et al. (2013) reported a mean Fe concentration of 2102 ± 608.9 ng m⁻³ in atmospheric TSP over the northern Yellow Sea based on shipborne sampling in spring 2007. Such differences might reflect interannual variability in atmospheric Fe concentrations over the Chinese marginal seas. This inference was supported by the model-simulated decline in dust-derived Fe transport from East Asia to the oceans during 2001–2017 (Zhu et al., 2025) and with the reported decrease in anthropogenic metals deposition in Chinese marginal Seas from 2012 to 2019 (Zhang et al., 2023a).

During the BY cruise, three high-Fe-concentration episodes (EP1, EP2, and EP3) were identified. These episodes were defined as periods during which Fe concentrations exceeded the 75th percentile of all samples collected during the cruise (218.2 ng m⁻³) and persisted for more than 12 hours. The spatial distribution and timing of these episodes are shown in Figs. 4a and 4b, respectively. EP1, EP2, and EP3 lasted 26.5, 16.5, and 23 hours, respectively (EP3 observations were truncated due to cruise termination), with corresponding mean Fe concentrations of 482.4 ± 537.8 ng m⁻³, 416.2 ± 90.54 ng m⁻³, and



320

325

330



906.2 ± 286.2 ng m⁻³. As shown in Fig. S4, the crustal element Ca exhibited trends similar to Fe during these episodes, with elevated Ca levels indicating dust influence. However, in EP1, the increase in Ca was markedly smaller than that of Fe, implying substantial contributions from non-dust sources. In contrast, pollution-related elements (Zn, Pb, and As) were abundant during EP1 and EP2 but occurred at very low levels during EP3, suggesting that EP3 represented a pure dust event. Satellite remote sensing and backward trajectory analyses confirmed that air masses during all three episodes originated from inland East Asia (Figs. S5 and S6), indicating that continental air masses transport can trigger rapid and substantial increases in marine atmospheric Fe concentrations. In particular, high-time-resolution measurements during EP3 recorded an approximately 13-fold increase in Fe concentration within just 9 hours, rising from 80.50 to 1111 ng m⁻³. This sharp rise coincided with a large-scale dust outbreak over northern China. According to the China Meteorological Administration (2022), this dust event affected Inner Mongolia, Ningxia, Gansu, Beijing, and Liaoning from April 25 to April 27, 2022. The subsequent transport of this dust-laden continental air mass to the Bohai Sea and Yellow Sea (Figs. S5e and S5f) played a dominant role in driving EP3.

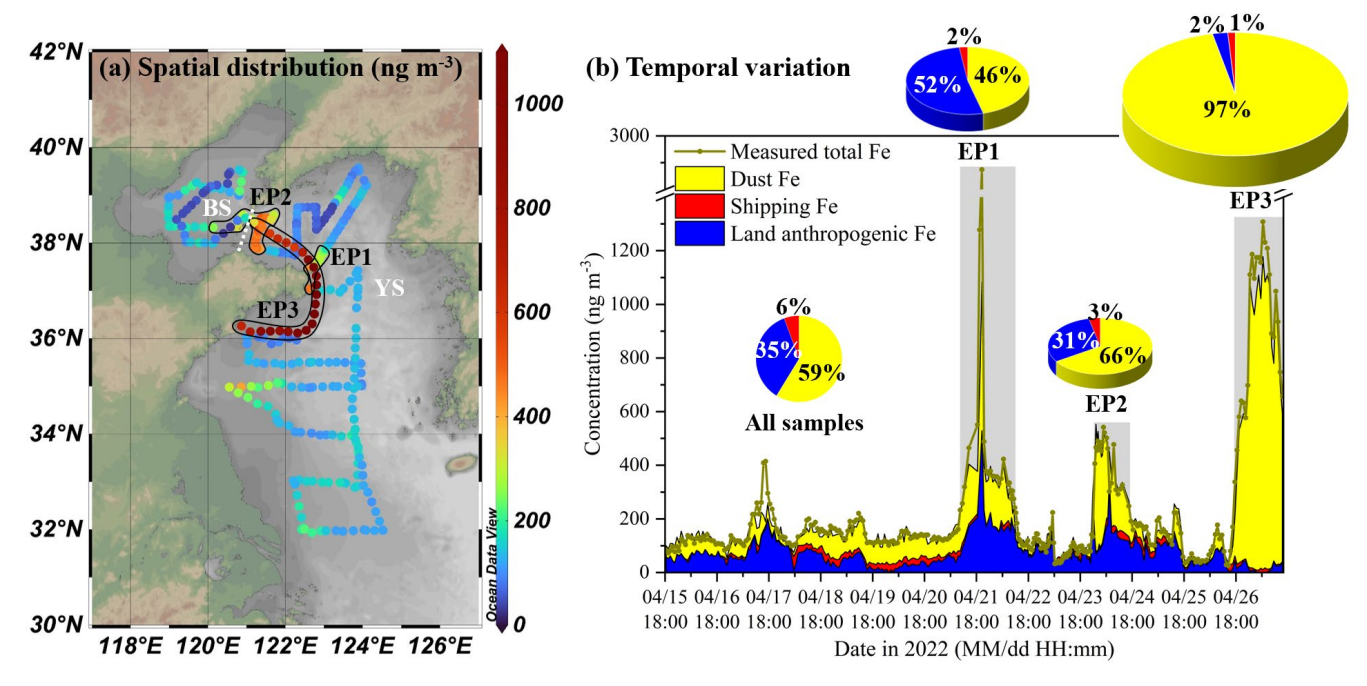


Figure 4. Spatiotemporal distribution of Fe concentrations in atmospheric PM₁₀ over the Bohai Sea and Yellow Sea in April 2022. (a) Spatial distribution of Fe concentrations. (b) Time series of measured total Fe and PMF-resolved Fe concentrations from different sources. EP1, EP2, and EP3 refer to three high-Fe-concentration episodes encountered during the observation period, whose spatial coverage and temporal ranges are indicated by black circles in (a) and shaded areas in (b), respectively. The four pie charts in (b) represent the proportion of Fe from different sources for the entire cruise and three episodes, respectively.

The PMF source apportionment results indicated that atmospheric Fe along the cruise tracks in Bohai-Yellow Sea primarily originated from dust sources (mean contribution was 59%), followed by land anthropogenic sources (35%), with



340

345

350

355



minimal input from ship emissions (6%). Fig. 4b shows temporal variations in Fe concentrations from different sources. Non-dust sources contributions were significant in most samples except during EP3. During the three episodes of elevated Fe concentrations, distinct source characteristics were identified. EP1 exhibited a mixed dust–anthropogenic signature, with the highest non-dust contributions to individual sample reaching 85% (mean was 54%). EP2 initially showed dust dominance, later shifting toward non-dust sources (mean of non-dust contributions was 34%). Conversely, EP3 was characterized by near-exclusive dust contributions (97%). Because these episodes were associated with continental air mass transport, the proportion of ship-derived Fe during the events decreased to 1–3%, below the cruise average (6%).

Fig. 5 shows the spatial distribution of Fe concentrations from different sources as determined by PMF analysis. Dust-derived Fe concentrations exhibited pronounced peaks during EP2 and EP3, reaching 283.5 ± 110.2 ng m⁻³ and 801.5 ± 283.6 ng m⁻³, respectively, while remaining much lower during other periods (55.71 ± 55.49 ng m⁻³). Excluding the EP events, dust-derived Fe concentrations were generally lower in the Bohai Sea and northern Yellow Seas than in the central and southern Yellow Sea (Fig. 5a). Although global model simulations have indicated that the meridional peak of East Asian dust transport to the ocean occurred near 40°N (Ito et al., 2019; Zhu et al., 2025), observations in this study showed higher dust-derived Fe concentrations in the Yellow Sea south of 37° N compared with those between 37° and 40° N. This result may represent a repeatable phenomenon. A previous study by Zhang and Gao (2007) examined the transport pathways of 42 Asian dust events and their impacts on the Chinese marginal seas. They reported that the Yellow Sea had the highest probability of dust influence at 31%, slightly higher than that of the Bohai Sea at 27%. Similarly, Jiang et al. (2024) used the CMAQ model to simulate dust-derived Fe concentration over Chinese marginal seas in 2017 and found higher values in the southern Yellow Sea than in the northern regions.

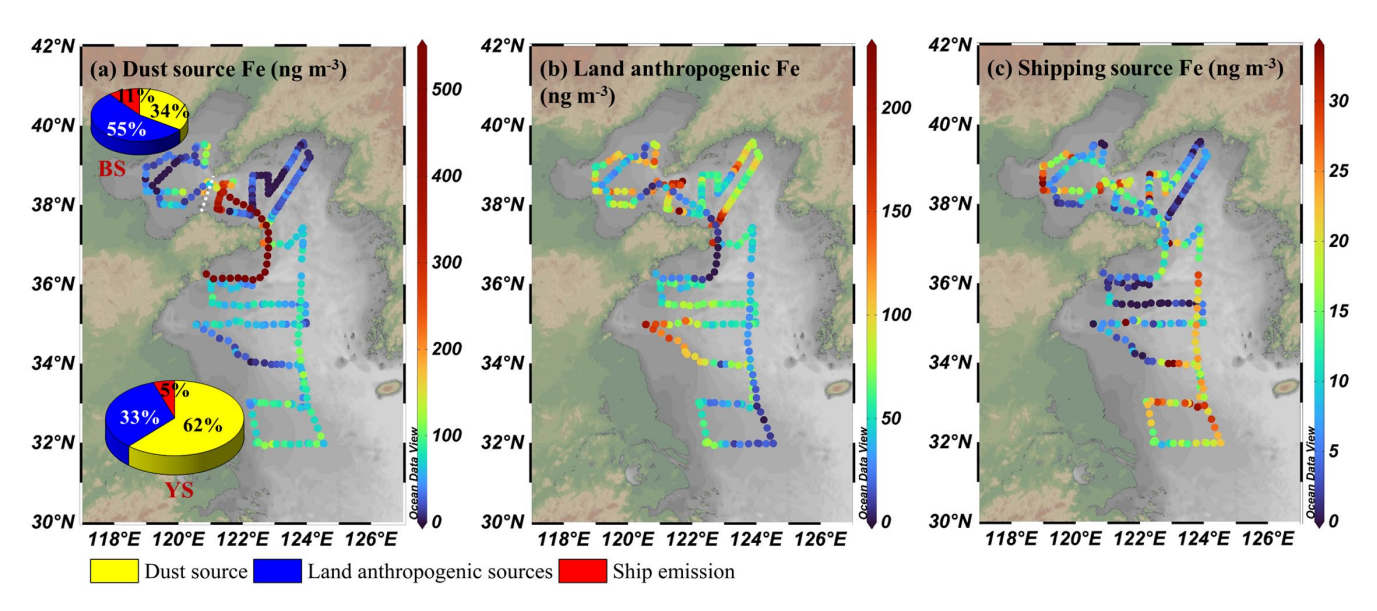


Figure 5. Spatial distributions of atmospheric Fe from different sources over the Bohai and Yellow Seas during the BY cruise. (a) Dust source Fe, (b) land anthropogenic source Fe, and (c) shipping source Fe. Pie charts in (a) show the mean percentage contributions of each source in the Bohai Sea (BS) and Yellow Sea (YS).



360

365

370

375

380

385



Unlike dust-derived Fe, non-dust sources, including land anthropogenic Fe (Fig. 5b) and ship-derived Fe (Fig. 5c), showed high concentrations in both the Bohai Sea and the Yellow Sea. The contrasting spatial distributions of Fe concentrations from different sources resulted in spatial variations of atmospheric source structures, with the non-dust contribution in the Bohai Sea (66%) higher than that in the Yellow Sea (38%) (Fig. 5a).

The spatial patterns of land anthropogenic Fe and ship-derived Fe also differed. High ship-derived Fe concentrations were observed mainly in the Bohai Sea and the southern Yellow Sea. The Bohai Rim and the Yangtze River Delta hosted major port clusters, and the rapid growth of maritime trade caused substantial ship emissions (Chen et al., 2017). As shown in Fig. S6, air mass back trajectories above the sampling area in southern Yellow Sea passed through the Yangtze River Delta, which explained the higher ship-derived Fe concentrations there.

In the central Yellow Sea, a south to north shipping route was associated with high ship-derived Fe concentrations during April 19–20. During this period, numerous vessels, predominantly small fishing boats, were observed within visual range of the research vessel (Fig. S7). Although previous source tests indicated that small fishing boats had lower V emission factors than ocean-going vessels (Zhang et al., 2018), such a dense cluster of emission sources around the research vessel was likely one reason for the elevated concentrations of V (14.27 ± 8.75 ng m⁻³) and ship-derived Fe (22.34 ± 4.82 ng m⁻³) recorded along this transect.

3.1.4 Sources of atmospheric total Fe in Northwest Pacific Ocean

Located downwind of East Asia, the Northwest Pacific is strongly influenced by continental aerosols outflow (Yu et al., 2020). To characterize atmospheric Fe in the region, we conducted two shipboard campaigns with online measurements (Fig. 1a). The first campaign (NWP1) was carried out in May–June 2021 and measured PM_{2.5} samples, and the second (NWP2) was conducted in June–July 2022 and measured PM₁₀ samples.

During the NWP1 cruise, Fe concentrations ranged from 2.60 to 401.7 ng m⁻³, with a median of 36.70 ng m⁻³ and a mean of 54.90 ± 52.48 ng m⁻³. Most high-Fe-concentration samples were clustered along the Yellow Sea and East China Sea (YES) leg (Fig. 6a). A few elevated values also appeared over the open Northwest Pacific, particularly in the mid-latitude oceanic area east of Japan between 37° and 39° N. A pronounced high-Fe-concentration episode occurred in this area from May 26 to May 28, with a peak of 401.7 ng m⁻³ (Fig. 6b). Similar with this phenomenon, our previous work reported two high-Fe-concentration events east of Japan during a spring 2015 cruise (Zhang et al., 2024), suggesting that this region served as an important receptor of continental aerosols outflow.

Source apportionment indicated that dust was the dominant contributor during NWP1, accounting for an average of 60% of total Fe, followed by land anthropogenic sources (37%) and ship emissions (3%). The non-dust contribution was higher in the YES region near the East Asian continent. During YES1 leg in May 2021, land anthropogenic sources and ship emissions contributed 48% and 4% on average, respectively, and during YES2 leg in June 2021, they contributed 52% and 16%, respectively. Overall, non-dust sources contributed 40% on average in NWP1 cruise, which was higher than our spring



400

405



2015 cruise result based on PM_{2.5} online measurements and PMF analysis (31%) (Zhang et al., 2024), and was also higher than the Fe-isotope-based estimate for PM_{2.5} samples reported by Kurisu et al. (2021) from two cruises in 2013–2014 (11% ± 4%). However, this value was lower than the modeled contribution of 59% simulated by CMAQ for the open Northwest Pacific in April 2017 (Jiang et al., 2024).

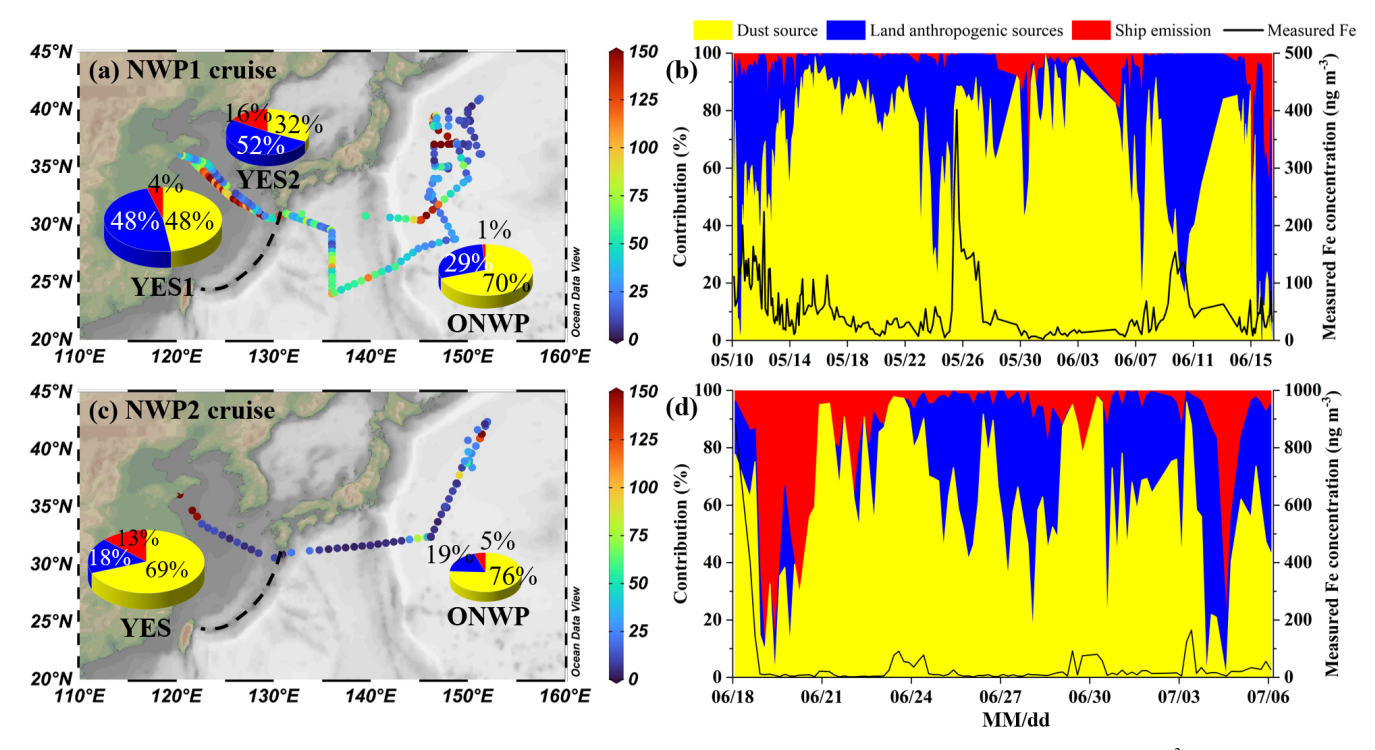


Figure 6. Concentration and sources of atmospheric total Fe over the Northwest Pacific. (a) Fe concentrations (ng m⁻³) in atmospheric PM_{2.5} during the NWP1 cruise in 2021. (b) Time series of Fe concentration and source composition during NWP1 cruise. (c) and (d) correspond to (a) and (b), respectively, but represent Fe in atmospheric PM₁₀ during the NWP2 cruise in 2022. The pie charts in (a) and (c) show the average source proportions of Fe for different sea areas. YES denotes the Yellow Sea and East China Sea, and ONWP denotes the open Northwest Pacific east of the black dashed line in (a) and (c).

During the NWP2 cruise, Fe concentrations ranged from 2.00 to 883.2 ng m⁻³, with a median of 10.58 ng m⁻³ and a mean of 35.56 ± 99.94 ng m⁻³. Although NWP2 collected PM₁₀ samples, both the mean and the median Fe concentrations were lower than those in PM_{2.5} samples in NWP1. High concentrations of 145.9-883.2 ng m⁻³ were recorded on the departure day, June 18, whereas subsequent samples along the Yellow Sea and East China Sea legs averaged only 7.97 ± 3.08 ng m⁻³, far below the values in YES region during NWP1 (76.35 ± 52.40 ng m⁻³). Meteorological observations on board indicated peak hourly rainfall intensities of 11.85, 8.30, and 30.9 mm/h on June 18, 19, and 20, respectively. Under the influence of precipitation, Fe concentrations dropped sharply to below 10 ng m⁻³. At the same time, PMF results showed a rapid decrease in the fractional contribution from dust and a relative increase in the contribution from ship emissions (Fig. 6d). These patterns indicated that wet deposition effectively scavenged atmospheric Fe, reducing the relative contribution of



425



continentally transported material while enhancing the relative influence of local emissions such as ship exhaust. Consequently, rainfall-induced wet deposition was the primary reason for the lower Fe concentrations observed along the subsequent YES leg during NWP2. Regarding sources, non-dust contributions in NWP2 were lower than in NWP1, averaging 27% over the entire cruise. Similarly, within NWP2, the coastal leg also showed a higher non-dust contribution (31%) than the open-ocean leg (24%) (Fig. 6c).

This study presents a further analysis of the causes of a high-Fe-concentration episode (EP) observed in the open Northwest Pacific Ocean during the NWP1 cruise. The episode, defined by Fe concentrations exceeding the 75th percentile (65.63 ng m⁻³) of the entire cruise dataset, persisted for approximately 48 hours. During this period, Fe concentrations rose sharply, increasing from 52.36 ng m⁻³ at 02:00 on May 26 (prior to the EP) to 401.7 ng m⁻³ at 10:00 on the same day (Fig. 7c), representing nearly a 7-fold increase within just eight hours.

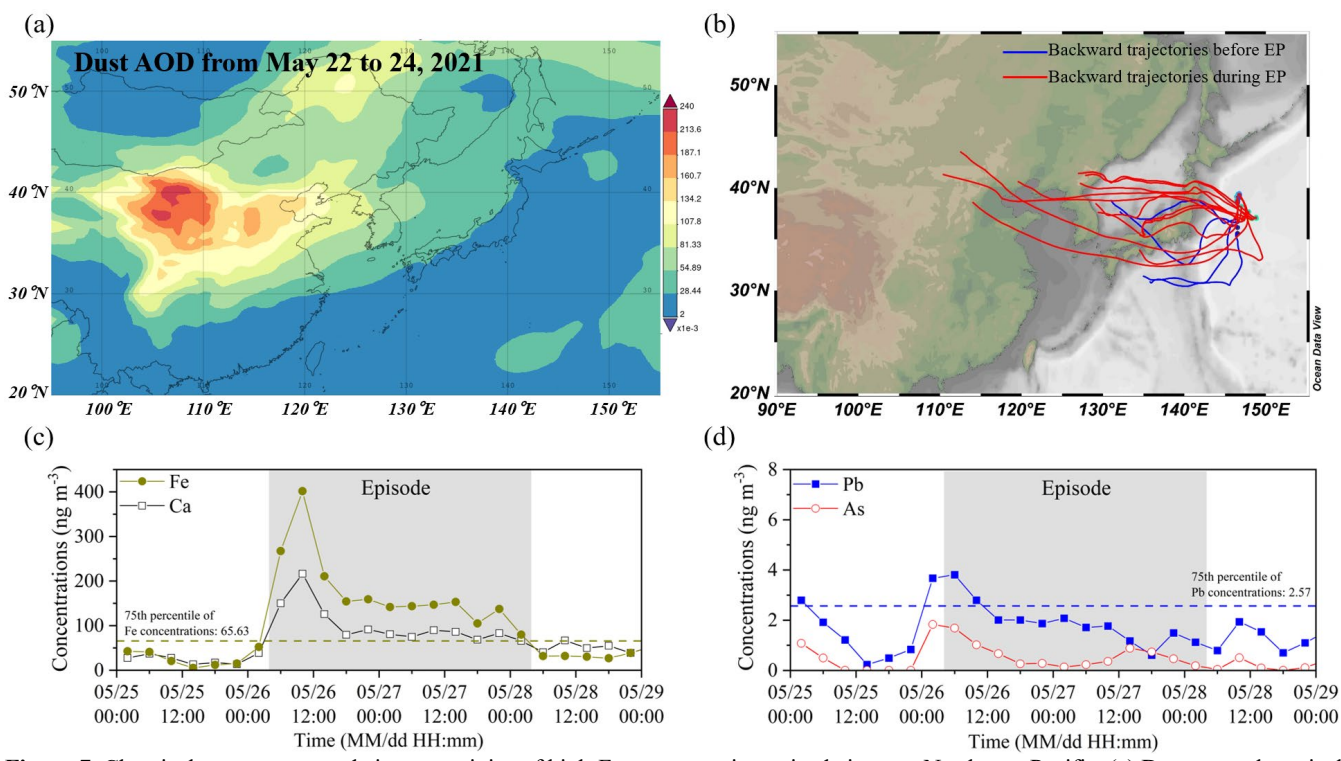


Figure 7. Chemical components and air mass origins of high-Fe-concentration episode in open Northwest Pacific. (a) Dust aerosols optical depth in east Asia during 22–24 May 2021, generated using the Giovanni online tool with MERRA-2 reanalysis data. (b) Seventy-two-hour backward air mass trajectories at 500 m altitude, with red lines representing trajectories during the high-concentration episode and blue lines representing those prior to the episode. (c) and (d) Variations in the concentrations of crustal elements (Fe, Ca) and pollution-derived elements (Pb, As) during and outside high-concentration episodes, respectively.

The episode was likely associated with a dust event in northern China. According to the Chinese Meteorological Bulletin of Atmospheric Environment, a dust event affected central-western Inner Mongolia, Ningxia, northern Shanxi, Hebei, Beijing, and Tianjin from May 22 to May 24 in 2021 (China Meteorological Administration, 2021). Dust aerosol



440

445

450

455

460



optical depth (AOD) data from the Modern-Era Retrospective analysis for Research and Applications, Version 2 (MERRA-2) for the same period revealed the spatial extent of dust aerosols during the event (Fig. 7a). Backward trajectory analysis showed that, before the episode, air masses over the sampling region originated mainly from oceanic areas south of Japan and the Sea of Japan, whereas during the episode they were predominantly from East Asian continent (Fig. 7b). This suggested that the long-range transport of dust-laden air masses from the continent was a significant contributor to the elevated Fe levels measured during the episode.

Compositional analysis of aerosols during the episode (Figs. 7c–7d) further supported this conclusion. Fe showed a similar variation pattern to Ca, a crustal element, indicating a substantial contribution from dust to the elevated Fe. During the episode, average Fe and Ca concentrations were 3.2 and 2.2 times their respective mean values in the entire cruise. In contrast, pollution-related elements such as Pb and As exhibited smaller fluctuations, with average concentrations of 1.87 ± 0.83 ng m⁻³ and 0.58 ± 0.45 ng m⁻³, corresponding to only 1.0 and 1.5 times their respective cruise means. PMF results further indicated that the dust source accounted for 79%–92% of Fe in samples collected during the episode (Fig. 6b). Collectively, these results demonstrate that the high Fe concentrations observed in the open Northwest Pacific during this episode were predominantly driven by dust particles, with non-dust sources playing a comparatively minor role.

3.2 Sources of soluble Fe in marine aerosols

3.2.1 Apportioning soluble Fe sources by integrating total Fe sources and Fe solubility

Drawing on previous experimental (Fu et al., 2012; Tang et al., 2023), observational (Sholkovitz et al., 2012; Shi et al., 2020), and modelling studies (Ito, 2015; Ito and Miyakawa, 2023), which collectively demonstrate that both source and atmospheric aging processes are pivotal in regulating Fe solubility in aerosols, this study posited that Fe solubility in ambient aerosols is principally determined by initial source characteristics and atmospheric processing. This dependence can be quantitatively described by Equation (3):

$$SFe\%_{i} = \sum_{j=1}^{n} (f_{i,j} \times SFe\%_{j,e}) + R$$
 (3)

where SFe%_i represents Fe solubility in ambient aerosols sample i; $f_{i,j}$ denotes the relative contribution of emission source j to total Fe content in sample i; SFe%_{j,e} indicates the initial Fe solubility from source j at emission; n is the number of source categories; and R accounts for atmospheric aging processes, including acid dissolution, photo-induced redox reactions, and organic ligand-mediated solubility changes (Ito et al., 2021), which are difficult to quantify directly in current observational research.

To resolve source-specific effects of atmospheric aging on Fe solubility, we decomposed the aging parameter R, as formalized in Equation (4). During transport from source regions to receptor sites, Fe from each emission source underwent atmospheric processing that increased its solubility. Equation (5) quantifies this enhancement of each source: SFe%_{j,e} represents the initial Fe solubility from source j at emission, while SFe%_{j,r} denotes Fe solubility at the receptor after



465

475

480

485



atmospheric processing. After obtaining SFe%_{j,r} from Equation (5), the calculation formula for Fe solubility in ambient aerosols samples is updated from Equation (3) to Equation (6).

$$R = \sum_{j=1}^{n} R_{j} \tag{4}$$

$$SFe\%_{j,r} = SFe\%_{j,e} + R_{j}$$
(5)

$$SFe\%_{i} = \sum_{j=1}^{n} \left(f_{i,j} \times SFe\%_{j,r} \right)$$
 (6)

Meanwhile, the relative contribution of source j to soluble Fe can be determined by combining total Fe sources and $SFe\%_{j,r}$, as expressed in Equation (7):

$$Sf_{i,j} = \frac{f_{i,j} \times SFe\%_{j,r}}{\sum_{j=1}^{n} (f_{i,j} \times SFe\%_{j,r})}$$
(7)

where $Sf_{i,j}$ denotes the contribution of source j to soluble Fe in sample i; $f_{i,j}$ represents the contribution of source j to total Fe in sample i; $SFe\%_{j,r}$ indicates the Fe solubility from source j at receptor following atmospheric aging.

In summary, two key inputs are required to determine the sources of soluble Fe using Equation (7). The first is the fractional contribution of each emission source to total Fe in the ambient sample $(f_{i,j})$, and the second is the source-specific Fe solubility at the receptor (SFe%_{j,r}). In this study, $f_{i,j}$ was obtained from the output of the PMF receptor model, and the determination and validation of SFe%_{j,r} are described in the next section.

3.2.2 Fe solubility parameterization and validation

Dust-source Fe solubility at receptor sites over oceanic regions was assessed by integrating observations from this study with those reported in previous literature. As described in Section 3.1.3, a severe dust event (EP3) occurred during the BY cruise, and the Fe solubility in the collected aerosols filter sample was 0.42%. Using Fe isotope source apportionment method, Kurisu et al. (2021) quantified total and soluble dust-derived Fe over the open Northwest Pacific and reported a dust-derived Fe solubility of 0.9%–1.3% in the marine atmosphere, higher than our measurements in the Chinese marginal seas. Similarly, Takahashi et al. (2011) observed that, during transport of an East Asian dust plume from northwestern China to Japan, Fe solubility increased from 0.28% to 1.1%. Integrating these findings, the solubility of dust-derived Fe in aerosols over Chinese marginal seas was set at 0.5% and that in the open Northwest Pacific was 1.0%.

Observational data on the solubility of anthropogenic Fe in marine aerosols remain limited. This study referenced the solubility of combustion-derived Fe (11%) reported by Kurisu et al. (2021), setting the solubility of land anthropogenic Fe at 11%. For ship emissions, which primarily originate from heavy oil combustion, the relatively short transport distance from ship emission sources to the receptors in marine atmosphere likely limited atmospheric aging. Therefore, we referred to



495

500

505



source test results for heavy oil combustion, including 38% (Desboeufs et al., 2001), 74.1% and 85.9% (Fu et al., 2012), 77% and 81% (Schroth et al., 2009). Based on these values, we assigned a ship-derived Fe solubility of 70%, a conservative value slightly below most source-test results. For subsequent calculations, we assumed spatially uniform solubilities for land anthropogenic Fe and ship-derived Fe across the study domain and applied the same values to both the Chinese marginal seas and the open Northwest Pacific.

Using the SFe%_{j,r} parameters defined above, Fe solubility of ambient samples from the three cruises was calculated with Equation (6). The calculated results were then compared with direct laboratory analysis of filters to validate the parameter settings. For the BY cruise, filter-based Fe solubility was compared with values calculated from online data. As shown in Fig. 8a, the two methods exhibited a strong linear correlation ($R^2 = 0.84$). Their ranges and mean values were also closely matched, with 0.42%–18.4% (mean $10.9\% \pm 5.4\%$) for the laboratory analysis and 1.8%–14.0% (mean $10.7\% \pm 4.2\%$) for the calculations. The overall mean difference was only 0.2 percentage points. Nevertheless, the measured values displayed greater variability than the calculated ones. For example, for samples BY3–BY6, measured solubility ranged from 11.5% to 18.4%, whereas the calculated values were more constrained (13.2%–14.0%). These samples were collected across the southern, central, and northern Yellow Sea (Fig. 1b), and the fluctuations in measured solubility likely reflected small-scale spatial variations in source-specific Fe solubility. Such variations in source-specific Fe solubility at fine spatial scales remain difficult to resolve fully in existing studies. Despite this limitation, the approach and the adopted SFe%_{j,r} parameters were considered acceptable for capturing regional mean values.

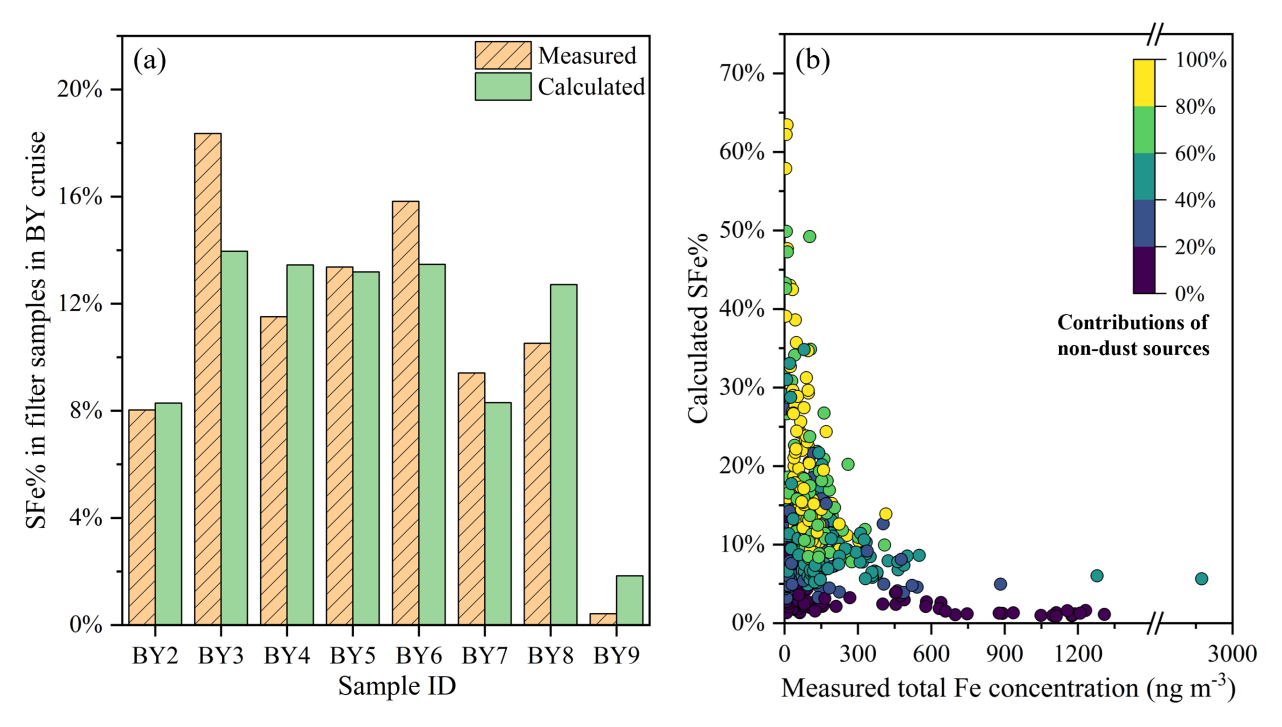


Figure 8. Validation of Fe solubility calculations. (a) Bar chart comparing measured and calculated Fe solubility for samples collected during the BY cruise; the BY1 filter sample was excluded because the online instrument data were incomplete



515

520

525

540



during its sampling period. (b) Scatter plot of calculated Fe solubility versus measured total Fe for all three cruises; point colour indicates the fraction of non-dust Fe (sum of land anthropogenic and ship-derived sources) in total Fe.

Across 644 online samples collected during the three cruises, the calculated Fe solubility ranged from 0.89% to 63.5%. This range was comparable to our previous estimate of 1.1% to 56.1% in the Northwest Pacific during spring 2015 (Zhang et al., 2024), and it was consistent with Sholkovitz et al. (2012), who reported Fe solubility of 132 samples in the North Pacific spanning from below 1% to greater than 50%. Moreover, a decline in Fe solubility with increasing total Fe mass concentration, as reported by Sholkovitz et al. (2012), was also observed in this study (Fig. 8b). This inverse relationship has been widely used in models to constrain simulations of soluble Fe in the marine atmosphere (Mahowald et al., 2018), which further supported the calculation approach adopted here.

Two complementary mechanisms have been proposed to explain the inverse relationship between Fe solubility and total Fe concentration. Baker and Jickells (2006) emphasized the role of atmospheric aging. During downwind transport, coarse particles are removed more rapidly by gravitational settling, leading to progressively lower total Fe concentrations and an increasing relative contribution of fine particles. The larger specific surface area of fine particles facilitated atmospheric chemical reactions, which enhanced Fe solubility in air masses with lower Fe concentrations. In addition, Sholkovitz et al. (2012) highlighted source effects. They posited that low Fe concentration plumes were dominated by high solubility combustion sources, whereas high Fe concentration plumes were dominated by low solubility dust emissions. Variable mixing of these plumes yielded the observed inverse relationship. Combing the PMF source apportionment, our results provided clear observational support for the latter interpretation. As shown in Fig. 8b, high solubility samples generally showed larger non-dust Fe fractions, whereas low solubility samples were typically dominated by dust-derived Fe.

3.2.3 Sources of atmospheric soluble Fe in Chinese marginal seas and the open Northwest Pacific

The Fe solubility, soluble Fe concentrations, and sources of soluble Fe for all online samples across the three cruises are presented in Fig. 9. Overall, the calculated Fe solubility in these samples ranged from 0.89% to 63.5%, with a median of 8.5% and a mean of 10.6% ± 8.8%. As shown in Figs. 9a to 9c, samples from the BY cruise exhibited relatively higher solubility, with a median of 11.3%, than the summer NWP2 cruise, with a median of 7.6%, and the spring NWP1 cruise, with a median of 5.0%. Across the three cruises, samples from the Chinese marginal seas mostly fell within the range from 5% to 25%, with the 10th percentile at 4.8% and the 90th percentile at 24.5%, whereas samples from the open Northwest Pacific primarily ranged from 2% to 12%, with the 10th percentile at 2.2% and the 90th percentile at 11.9%. The Mann Whitney U test indicated a statistically significant difference in Fe solubility between coastal and open ocean samples (*p* < 0.01).

This result differed from previous global model simulations. Using the IMPACT model, Ito et al. (2021) reported that, within the spatial domain of our study, atmospheric Fe solubility over the Chinese marginal seas (2%–4%) was slightly lower than that over the open Northwest Pacific (4%–6%). Hamilton et al. (2019), employing the CMA model, reported Fe solubility of 4%–6% for both regions. Moreover, when atmospheric aging mechanisms were incorporated, the models



555



generally simulated elevated Fe solubility over the remote ocean rather than in coastal regions (Mahowald et al., 2018; Ito et al., 2021). Nevertheless, across the study domain, model-simulated Fe solubility was consistently lower than our results, especially in the Chinese marginal seas. This shortfall likely reflects the models' underestimation of non-dust emissions contributions in regions strongly influenced by human activities.

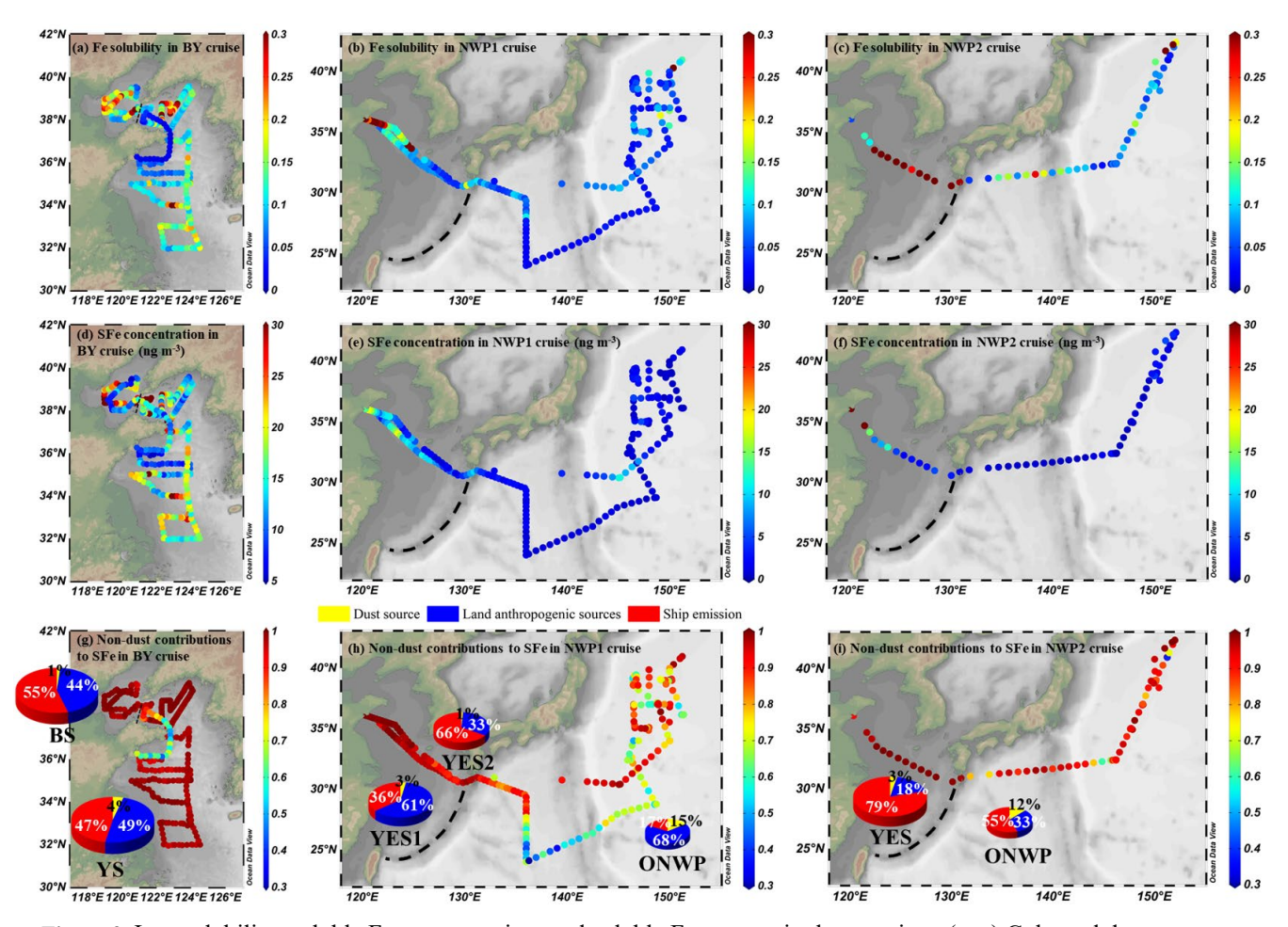


Figure 9. Iron solubility, soluble Fe concentration, and soluble Fe sources in three cruises. (a–c) Coloured dots represent atmospheric Fe solubility (unitless) for the BY cruise, NWP1 cruise, and NWP2 cruise, respectively. (d–f) Coloured dots represent atmospheric soluble Fe concentrations (ng m⁻³) for the three cruises, respectively. (g–i) Coloured dots represent the fractional contribution of non-dust sources to soluble Fe (unitless), respectively. Pie charts in (g–i) depict the average contributions of different sources to soluble Fe in different cruise legs.

The calculated atmospheric soluble Fe concentrations for each cruise are shown in Figs. 9d-9f. The soluble Fe concentrations across the three cruises spanned from 0.15 to 61.29 ng m⁻³. The data indicated a more rapid decline in soluble Fe mass concentrations from the Chinese marginal seas to the open Northwest Pacific Ocean than the corresponding decrease in Fe solubility. The 10th to 90th percentile range for soluble Fe concentration in coastal samples was 6.60–26.44



560

565

570

575

580

585

590



ng m⁻³, contrasting sharply with 0.39–3.21 ng m⁻³ for the open northwest Pacific samples, representing a difference exceeding one order of magnitude. Such a nearshore-to-offshore decline in soluble Fe concentrations (or deposition fluxes) has been captured by most model studies (Hamilton et al., 2020; Rathod et al., 2020; Ito et al., 2021). In particular, Rathod et al. (2020) using the CAM model and a newly developed anthropogenic Fe emission inventory, simulated soluble Fe concentrations of 10–100 ng m⁻³ over the Chinese marginal seas, which were higher than the 1–10 ng m⁻³ over the open Northwest Pacific. These results showed relatively high comparability with those from the present study.

Source apportionment of atmospheric soluble Fe was conducted using Equation (7). Coloured dots in Figs. 9j–9i indicate the fractional contributions of non-dust sources, comprising land anthropogenic emissions and ship emissions, to soluble Fe. The results showed that non-dust sources accounted for more than 90% of soluble Fe in most samples during the observation period. In the Chinese marginal seas, mean contributions from non-dust sources reached 96%–99% across five coastal cruise legs (BS and YS legs in BY cruise; YES1 and YES2 legs in NWP1 cruise; YES leg in NWP2 cruise). In contrast, contributions decreased over the open Northwest Pacific Ocean with increasing distance from the East Asian continent. For example, mean contributions declined to 85% and 88% in the ONWP legs of the NWP1 and NWP2 cruises, respectively.

The trend of higher contributions from non-dust sources to soluble Fe in coastal regions than in open ocean has also been captured by most models. However, the specific contribution values vary considerably among studies due to differences in emission inventories and atmospheric chemical processing schemes. For example, Wang et al. (2015) reported that non-dust sources (combustion-related) accounted for more than 95% of soluble Fe deposition in Chinese marginal seas and over 85% in the open Northwest Pacific. In comparison, Ito et al. (2019) simulated contributions exceeding 80% and 70% for these two regions, respectively. Lower estimates have also been reported, such as 40%–60% when considering anthropogenic sources alone (Matsui et al., 2018), and 20%–60% when anthropogenic and wildfire sources were combined (Rathod et al., 2020).

In addition to the zonal gradient, a pronounced meridional variation was also observed in the open Northwest Pacific. During the NWP1 cruise, the contribution of non-dust sources to atmospheric soluble Fe concentrations was lower in low-latitude regions. For samples collected south of 26° N, the non-dust contribution averaged $49.5\% \pm 10.8\%$ (Fig. 9h). Some models have reproduced such meridional variations in non-dust contributions (Lin et al., 2015; Wang et al., 2015), whereas others have shown little or no such pattern in this region (Matsui et al., 2018; Ito et al., 2019).

Both land anthropogenic emissions and ship emissions exerted substantial influences on marine atmospheric soluble Fe. During the BY cruise, contributions from these two sources were comparable, with ship emissions slightly exceeding land anthropogenic contributions in the Bohai Sea (Fig. 9g). In comparison, shipping contributions markedly exceeded those from land anthropogenic sources during the YES2 leg of the NWP1 cruise and the YES and ONWP legs of the NWP2 cruise (Figs. 9h and 9i). As these three legs took place in June–July, this may indicate that the contribution of ship emissions to marine atmospheric soluble Fe increases markedly in summer. This pattern was probably attributable to the suppression of land-derived aerosols transport to the ocean by the East Asian Summer Monsoon (southwesterly to southerly winds), which in



595

600

605

610

615

620



turn enhanced the relative contribution from local ship emissions. In addition, Jiang et al. (2024) reported that metal emissions from ships in this region were higher in summer than in spring, which may also contribute to the observed seasonal variations. Collectively, these findings indicate that the sources of marine atmospheric soluble Fe exhibit not only spatial differences but also temporal variability (Hamilton et al., 2020).

3.3 Spatiotemporal variations of Fe sources

3.3.1 Spatial distribution of Fe concentration from different sources

Across all cruises, atmospheric total Fe concentrations generally ranged from 10 to 300 ng m⁻³ (10th–90th percentile: 10.17–300.4 ng m⁻³), while dust-derived Fe, identified via PMF analysis, ranged from 3 to 130 ng m⁻³ (10th–90th percentile: 2.61–128.4 ng m⁻³). Total Fe and dust-derived Fe exhibited broadly similar spatial patterns (Figs. 10a and 10c), with higher values in the Bohai and Yellow Seas, along with sporadic elevated values detected in open-ocean regions east and south of Japan. The highest levels occurred near the Shandong Peninsula during a major dust event (EP3, detailed in Section 3.1.3) during the BY cruise, when mean dust-derived Fe reached 801.5 ± 283.6 ng m⁻³, which was nearly 17 times the average of other samples (47.45 ± 67.04 ng m⁻³). Consequently, dust-derived Fe concentrations in the YS leg of the BY cruise were significantly higher than in other legs (Fig. 10d). Notably, even after excluding EP3, the average dust-derived Fe concentration over the Yellow Sea (76.69 ± 88.36 ng m⁻³) still exceeded those in other legs (13.70–62.49 ng m⁻³), indicating the Yellow Sea's role as an important outflow pathway for East Asian dust to the Northwest Pacific.

The comparisons of Fe concentration gradients between the Chinese marginal seas and the open Northwest Pacific during the same cruise showed that, in NWP1 cruise, the average concentrations of total Fe and dust-derived Fe over coastal waters were approximately 1.6 and 1.1 times higher, respectively, than those in the open ocean. These contrasts were less pronounced than model simulations. For example, Zhu et al. (2025) using the CAM model to simulate spring dust concentrations for 2015–2017, reported dust mass concentrations of 20–60 μg m⁻³ over the Bohai and Yellow Seas, markedly higher than the 5–20 μg m⁻³ over the open Northwest Pacific. A likely explanation for the weaker gradient during NWP1 cruise in this study is the prevailing East Asian summer monsoon, which transported most air masses over the sampling region from the oceanic regions rather than the continent (Fig. S8), thereby limiting dust input from East Asia. In comparison, during NWP2 cruise, the nearshore-offshore differences in both total Fe and dust-derived Fe were more pronounced. This enhancement was largely driven by three high-Fe-concentration samples collected during the early phase of the YES leg, which substantially elevated mean values in coastal area. Back trajectory analysis indicated that these samples were influenced by air masses originating from inland and eastern coastal China (Fig. S8b). In the later phase of the YES leg, air masses shifted to predominantly marine origins over the East China Sea. Meanwhile, precipitation events contributed to a rapid decline in both total and dust-derived Fe concentrations, reducing them to levels even lower than those observed in the open Northwest Pacific (Fig. 6d).



630

640



During the three cruises, substantial amounts of land anthropogenic Fe were detected in the marine atmosphere, typically ranging from 1 to 100 ng m⁻³ (10th–90th percentile: 1.12-106.8 ng m⁻³). Compared with dust-derived Fe, land-anthropogenic Fe showed greater variability among cruises. As shown in Fig. 10e, concentrations during the BY cruise were significantly higher than those during the Northwest Pacific cruises. Similar to dust-derived Fe, occasional high concentrations were also observed over open-ocean regions. For example, during the NWP1 cruise, persistently elevated levels (66.19-104.5 ng m⁻³) were recorded southeast of Japan for approximately 32 hours. These samples were notably enriched in pollution-related elements such as As, Zn, and Pb, reaching 4.5, 3.5, and 2.7 times the cruise averages, respectively, suggesting substantial influence from coal combustion and industrial emissions on land. Cruise-leg comparisons (Fig. 10f) show that land anthropogenic Fe concentrations were significantly higher in the Bohai Sea (72.34 ± 39.97 ng m⁻³) and Yellow Sea (75.70 ± 60.79 ng m⁻³) legs than in other legs. In both Northwest Pacific cruises, pronounced contrasts were observed between the coastal and open-ocean legs. During NWP1, the mean land anthropogenic Fe concentration in the YES leg was 3.0 times higher than that in the ONWP leg, and during NWP2 the difference increased to 4.7 times.

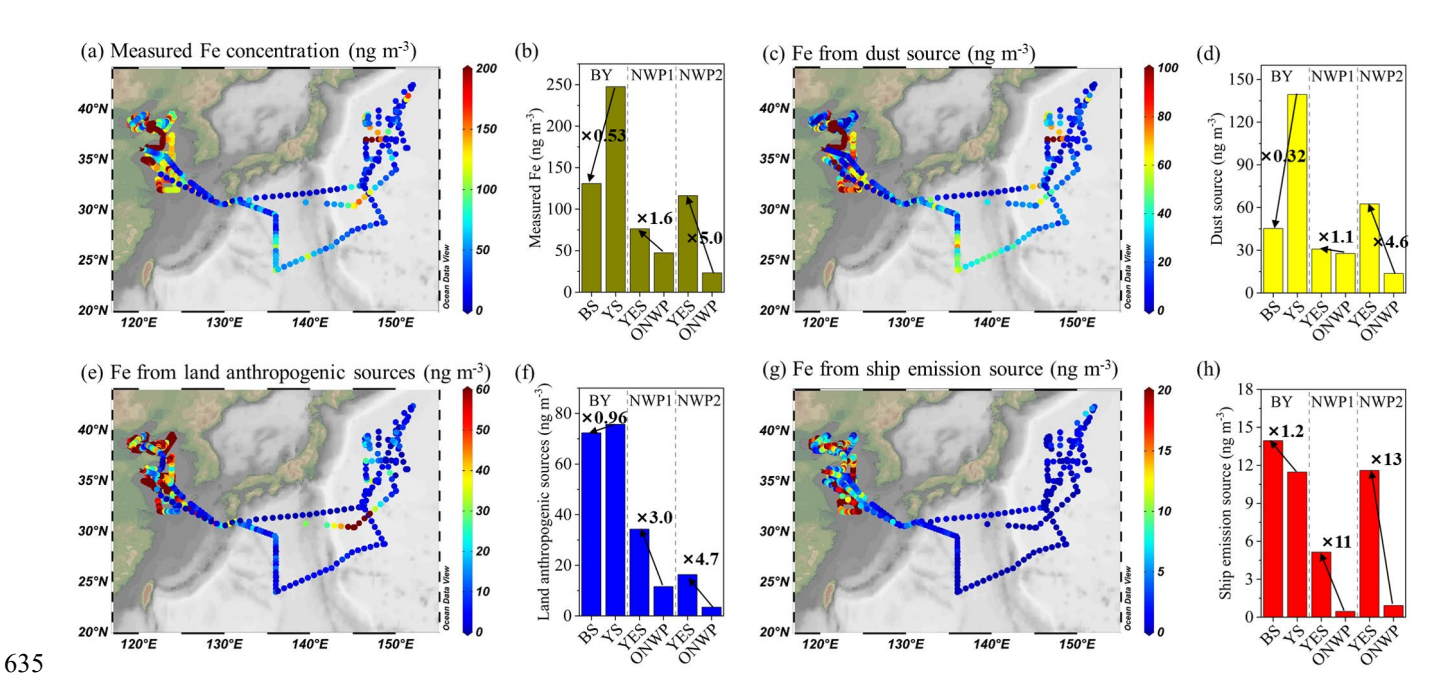


Figure 10. Spatial distribution of Fe concentrations from different sources. (a), (c), (e), (g) represent spatial distributions of measured total Fe, and PMF-resolved dust Fe, land anthropogenic Fe, and shipping Fe concentrations, respectively. (b), (d), (f), (h) represent mean concentrations of the corresponding Fe categories for different cruise legs, respectively; the three cruises are separated by dashed lines. Arrows and labels between bars indicate multiples of concentration differences between legs within the same cruise.

As shown in Fig. 10g, Fe concentrations from ship emissions were generally much lower than those from other sources, typically below 20 ng m⁻³ (10th–90th percentile: 0.01–20.04 ng m⁻³). Unlike land-based dust and anthropogenic emissions,



645

650

655

660

665

670

675



ship emissions originate in marine areas and are primarily concentrated around ports and along major shipping routes (Chen et al., 2017; Johansson et al., 2017; Zhang et al., 2017). Consequently, the spatial variability in ship emission intensity over the ocean likely exerts a strong influence on the spatial distribution of ship-sourced Fe concentrations in marine aerosols. Source apportionment results from the three cruises indicate that elevated concentrations of shipping Fe were primarily observed in legs within the Chinese marginal seas (Fig. 10g), reflecting the high density of maritime traffic in these regions. The coastal sampling tracks in this study were located near more than a dozen major ports, including Dalian, Yingkou, Qinhuangdao, Tangshan, Tianjin, Huanghua, Yantai, Qingdao, Rizhao, Lianyungang, Nantong, and Shanghai (Chen et al., 2017). Ship emissions in these port areas, as well as along the shipping lanes connecting them, contributed substantially to ship-sourced Fe, resulting in generally high concentrations in coastal legs. Mean ship-sourced Fe concentrations across different legs in marginal seas ranged from 5.15 to 13.95 ng m⁻³ (Fig. 10h). These values were higher than those simulated by Jiang et al. (2024) using the CMAQ model, which estimated ship-sourced Fe concentrations in the Bohai and Yellow Seas at around 3 ng m⁻³, with high-concentration zones exceeding 6 ng m⁻³. However, the average concentrations observed in our two open-ocean legs (0.46 and 0.92 ng m⁻³) were comparable to Jiang's simulation results for these regions, which were generally below 1 ng m⁻³.

Compared to dust-derived and land anthropogenic Fe, ship-sourced Fe exhibited a much sharper nearshore-offshore gradient. As shown in Fig. 10h, during NWP1 cruise and NWP2 cruise, the YES legs exhibited ship-sourced Fe concentrations up to 11 and 13 times higher, respectively, than those in the corresponding open-ocean legs. This pattern was consistent with spatial differences in ship emission intensities. For example, the ship emission inventory of Johansson et al. (2017) indicates that PM_{2.5} emissions from ships in the Chinese marginal seas were several tens of times higher than those in the open Northwest Pacific east of Japan.

To further evaluate the relative influence of sampling region and season on Fe concentrations from different sources, we applied the Scheirer-Ray-Hare (SRH) test, a nonparametric two-way ANOVA analogue based on ranked data (Scheirer et al., 1976). In this analysis, sea area (Chinese marginal seas versus the open Northwest Pacific) and season (spring versus summer) were treated as two independent factors (Table 1). The SRH test yields H values, which represent the magnitude of the factor's effect, with larger H values indicating stronger influence.

As shown in Table 1, the factor of sea area exerted statistically significant effects (p < 0.01) on Fe concentrations from all three sources, although the H-value for dust-derived Fe was much lower than that for non-dust sources. The weaker spatial variability of dust-derived Fe compared with non-dust sources has been discussed above and has also been reported in model simulations (Jiang et al., 2024). This is likely because Asian dust storms are frequently associated with strong synoptic systems such as Mongolian cyclones, cold fronts, and cold highs, which can lift dust particles to altitudes of several kilometers and promote long-range transport (Meng et al., 2019; Yin et al., 2022; Zhang et al., 2023b). As a result, dust-derived Fe can be carried to remote oceanic regions, producing weaker spatial gradients than non-dust Fe, whose transport distances are more limited.



685

690

695

700

705



Table 1. Scheirer-Ray-Hare test results of Fe concentrations from different sources

Variables	H-value (Sea area)	H-value (Season)	H-value (Sea area × Season)
Dust source Fe concentrations	$14.20 \ (p < 0.01)$	77.82 (<i>p</i> < 0.01)	8.68 (<i>p</i> < 0.01)
Land anthropogenic Fe concentrations	155.47 (<i>p</i> < 0.01)	32.19 (p < 0.01)	27.56 (p < 0.01)
Shipping Fe concentrations	235.07 (<i>p</i> < 0.01)	0.14 (p = 0.71)	3.34 (p = 0.07)

^{*}The table presents the main effects of sea area (i.e., Chinese marginal seas or the open Northwest Pacific) and season (i.e., spring or summer) on the concentrations of Fe from various sources, as well as their interaction effects;

In contrast, the factor of season had its strongest influence on dust-derived Fe concentrations compared with non-dust sources. This is attributable to the pronounced seasonality of East Asian dust emissions, particularly the contrast between spring and summer. The marked seasonal variability of dust-derived Fe over the Northwest Pacific, with higher concentrations in spring and lower values in summer, has been well documented in previous studies (Lin et al., 2015; Hamilton et al., 2020). It was further noted that seasonal effects were significant for dust and land anthropogenic sources but not for ship-derived Fe. This likely reflects the strong influence of seasonal meteorological conditions on the transport of terrestrial emissions to the ocean. The pronounced seasonal shifts of the East Asian monsoon, with prevailing northwesterly winds in spring and southwesterly to southerly winds in summer, modify transport pathways and thereby increase the seasonal sensitivity of land-based Fe inputs relative to those from local ship emissions. Moreover, the interaction effects between factors of sea area and season were significant for both dust and land anthropogenic Fe concentrations, indicating that the influence of season on Fe levels varies across regions and that regional contrasts vary with season.

3.3.2 Source structure of atmospheric total Fe and soluble Fe across different sea areas and seasons

The differing spatial patterns of Fe concentrations from various sources lead to marked spatial variability in the source structure of Fe in marine aerosols. To examine the combined influence of sea area and season, the 644 online samples from the three cruises were classified into four groups: spring samples from the marginal seas (n = 349), summer samples from the marginal seas (n = 41), spring samples from the open Northwest Pacific (n = 116), and summer samples from the open Northwest Pacific (n = 138).

The source structure of atmospheric total Fe in individual samples is shown in Fig. 11a. Most samples are distributed between the vertices representing land anthropogenic sources and dust source, indicating that these two sources were the dominant contributors to total Fe during the observation period. Samples from the open Northwest Pacific generally plot closer to the dust-source vertex than those from the marginal seas, particularly in spring (green solid circles in Fig. 11a), with most falling to the right of the yellow diagonal line in Fig. 11a, indicating a dust contribution exceeding 50%. In contrast, ship emission contributions to total Fe were generally low (< 25%). Samples with ship source contributions above 25% were

^{**}A p-value less than 0.01 indicates that the factor has a significant effect on the variable, while the magnitude of the H-value reflects the strength of that effect.



715

720



mainly collected in coastal regions (triangles in Fig. 11a). Notably, among the 11 samples with ship contributions exceeding 50%, nine were collected in marginal seas during summer (left of the red diagonal line in Fig. 11a), highlighting the elevated relative contribution of ship emissions in coastal waters during summer when dust and land anthropogenic Fe concentrations were reduced.

In comparison, Fig. 11c illustrates the source structure of atmospheric soluble Fe in individual samples. Most sample points are located between the vertices representing land anthropogenic sources and ship emissions, indicating that soluble Fe during the observation period was primarily derived from non-dust sources. Samples with dust-source contributions exceeding 25% were primarily collected from the open Northwest Pacific in spring, with a few additional samples originating from the same region in summer and from coastal areas in spring.

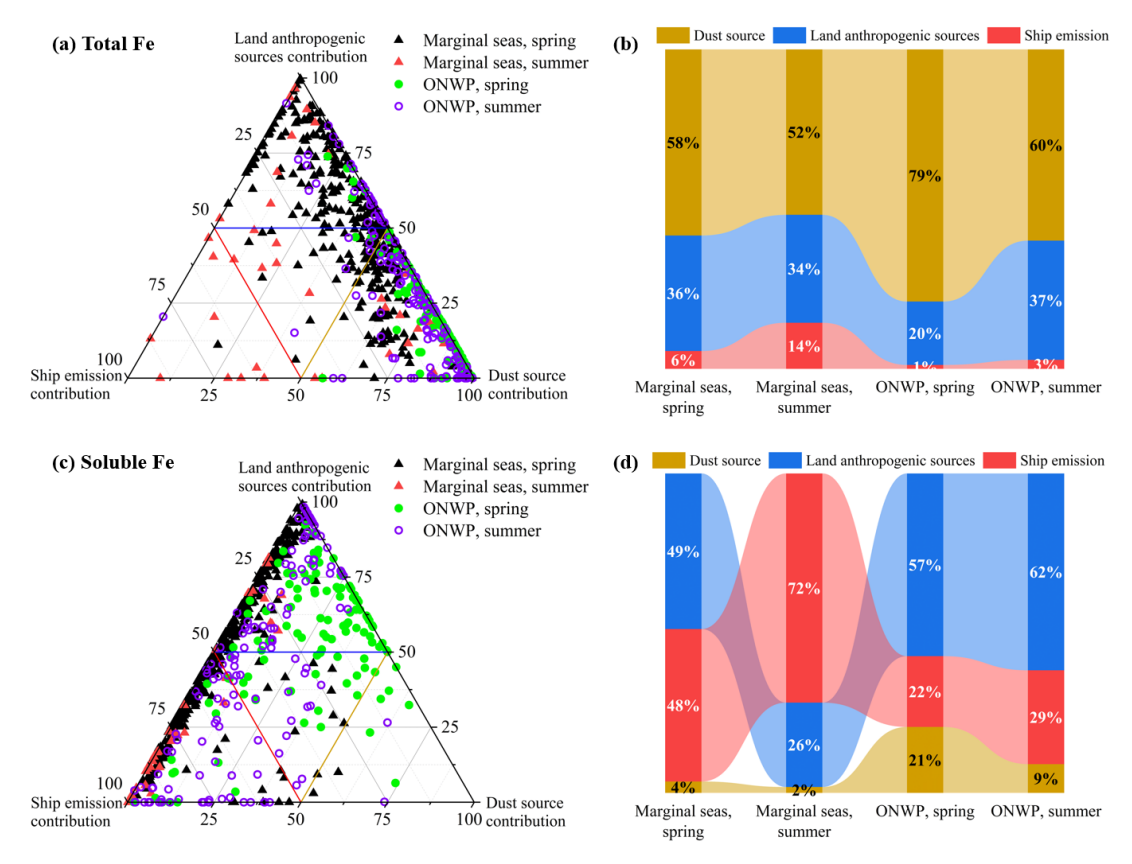


Figure 11. Source structure of total Fe and soluble Fe across different sea areas and seasons. (a) and (c) are ternary plots illustrating the source structure of total Fe and soluble Fe, respectively; the three vertices represent the three sources; the closer a sample point is to a given vertex, the greater the relative contribution of that source to the sample. (b) and (d) show the average contributions of the three sources to total Fe and soluble Fe, respectively, across different sea areas and seasons.

The average source structure of total Fe and soluble Fe for each group are shown in Figs. 11b and 11d. Overall, there was a consistent pattern showing that non-dust sources contributed more to both total and soluble Fe in coastal regions than



725

730

735

740

745

750

755



in open-ocean areas, and more in summer than in spring. As shown in Fig. 11b, dust remained the dominant source of total Fe, accounting for an average of 52%–79% across the groups. Its contribution was particularly high in the open Northwest Pacific, reaching nearly 80% in spring and about 60% in summer. Land anthropogenic emissions represented a relatively stable non-dust source for total Fe, contributing 20%–37% on average. In contrast, ship emissions contributed less to total Fe, ranging from 6% to 14% in coastal areas and remaining below 5% in open-ocean regions.

For soluble Fe, however, dust made the smallest contribution, averaging only 2%–21% across the groups (Fig. 11d). Non-dust sources dominated atmospheric soluble Fe throughout the study area, with both land anthropogenic and ship emissions making substantial contributions in coastal regions. Notably, in the summer coastal group, ship emissions became the largest contributor to soluble Fe, accounting for 72%. In the open Northwest Pacific, land anthropogenic sources dominated, contributing 57%–62%. The predominance of ship emissions as the main source of soluble Fe in coastal regions during summer can be attributed to two main factors. First, intensive shipping activity in Chinese marginal seas results in relatively high absolute concentrations of ship-derived Fe (Fig. 10g). Second, increased precipitation during summer suppresses dust emissions, and the East Asian summer monsoon reduces the transport of aerosols from land to sea. Backward air mass trajectories for coastal summer samples (Fig. S9) indicated that most air masses originated from oceanic areas, including Yellow Sea, East China Sea, and southern Sea of Japan. Previous modeling and observational studies have also emphasized the importance of ship emissions in contributing to atmospheric soluble Fe in specific regions and seasons. For example, Ito (2013) reported that under low Asian dust conditions, ship emissions could account for up to 40% of soluble Fe deposition over the Northeast Pacific in summer based on model simulations. Based on observations from the eastern coastal region of South Korea, Seo and Kim (2023) found that ship emissions contributed as much as 45% of atmospheric soluble Fe concentration.

Given the significant reductions in land anthropogenic emissions and coastal ship emissions resulting from China's recent air pollution control policies (Zhang et al., 2019; Dong et al., 2025), along with the interannual variability of dust activity (Tai et al., 2021; Zhu et al., 2025), the future source structure of atmospheric total Fe and soluble Fe over the ocean remains uncertain. Therefore, more observations, particularly from shipborne measurements, are essential for improving our understanding of real-world changes in the marine atmosphere. Such data are also critical for optimizing atmospheric models and providing accurate inputs to ocean biogeochemical models to assess the environmental impacts of atmospheric composition changes.

4 Summary and conclusions

This study provides a comprehensive assessment of the sources and spatiotemporal variability of atmospheric Fe over the Chinese marginal seas and the open Northwest Pacific Ocean, based on shipborne high-time-resolution measurements from three observation campaigns. Our results demonstrate that dust remains the most important contributor to total Fe, particularly in the open ocean during spring, whereas non-dust sources (including land anthropogenic sources and ship



760

765

770

775

780

785



emissions) are the primary contributors to soluble Fe, especially in coastal regions and during summer. While dust Fe concentrations showed stronger seasonal variability, non-dust Fe concentrations responded more strongly to spatial (coastal versus offshore) differences. For instance, the average concentration of land anthropogenic Fe in the Chinese marginal seas was 3–5 times higher than in the open Northwest Pacific during the same cruises, and shipping Fe showed even greater contrasts, with coastal concentrations exceeding open Northwest Pacific values by more than an order of magnitude.

In terms of source structure, non-dust sources accounted for 21%–48% of total Fe and 79%–98% of soluble Fe across different regions and seasons. Among these, land anthropogenic sources contributed substantially to both total Fe (20%–37%) and soluble Fe (26%–62%). In contrast, the contribution of ship emissions to total Fe was relatively minor, particularly in open ocean regions (< 5%), yet it represented a notable source of soluble Fe, accounting for 22%–72%. Overall, the relative contributions of non-dust sources to both total and soluble Fe were generally higher in coastal regions than in the open ocean, and higher in summer than in spring. In open Northwest Pacific areas, land anthropogenic emissions were the dominant source of atmospheric soluble Fe. In coastal regions, the influence of ship emission source was enhanced, and during summer it surpassed land anthropogenic sources as the dominant contributor to atmospheric soluble Fe, accounting for up to 72%.

Methodologically, this study validated and advanced approaches for atmospheric Fe source apportionment in marine environment. By comparing PMF-resolved source-specific total Fe derived from online measurements with traditional filter-based chemical tracers, we confirmed the utility of Al as a reliable tracer for dust-derived Fe in marine atmosphere, particularly during intense dust events. However, our results also highlight that dust-associated elements can interfere with the source attribution of tracers for non-dust sources by increasing their concentrations, particularly evident for V, and to a lesser extent for Pb. We further estimated Fe solubility and apportioned soluble Fe sources using empirical solubility factors assigned to different sources. These estimates showed strong agreement with laboratory-based solubility measurements from filter samples ($R^2 = 0.84$), supporting the robustness of the proposed parameterization approach. In addition, comparison with previous modeling studies suggests that some models may underestimate high solubility of Fe in Chinese marginal seas and may have limitations in capturing the meridional variation of soluble Fe sources over the open Northwest Pacific.

Overall, the findings highlight the important role of non-dust sources in shaping the bioavailable Fe pool in the marine atmosphere, particularly during summer when dust input is reduced and in marginal seas where non-dust emissions are more active. The distinct spatial and seasonal variations in Fe sources revealed in this study provide valuable observational constraints for improving Fe deposition models, and offer new insights into the biogeochemical impacts of land anthropogenic and ship emissions on marine ecosystems.

Data availability

The data used in this study are available from the corresponding authors upon request (mzheng@pku.edu.cn).





Author contributions

TZ: investigation, formal analysis, writing-original draft. YX: methodology, visualization. BZ: investigation, methodology. XY: investigation, methodology. XF: writing-review and editing. YW: methodology. YW: writing-review and editing. SC: methodology. YZ: investigation, methodology. FC: methodology. MZ: conceptualization, funding acquisition, methodology, supervision.

Competing interests

The contact author has declared that neither they nor their co-authors have any competing interests.

795 Acknowledgements

Data and samples were collected aboard R/V *Lanhai 101* during the open research cruise NORC2022-01, and aboard R/V *Dongfanghong 3* operated by the Ocean University of China. We thank the crews of both vessels, as well as Dr. Dihui Chen and Dr. Yating Gao, for their assistance with the shipboard observations. We are also grateful to Prof. Tong Zhu from Peking University and Dr. Tinghao Sun from the Undergraduate Laboratory Teaching Center, College of Environmental Sciences and Engineering, Peking University, for providing the Xact 625 and TH-16A sampling equipment, respectively.

Financial support

This work was sponsored by the National Natural Science Foundation of China (42030708), Key Technologies Research and Development Program of China (No. 2022YFC3702602), and the Postdoctoral Fellowship Program of China Postdoctoral Science Foundation (GZC20250890).

805 References

- Alexander, B., Park, R. J., Jacob, D. J., and Gong, S.: Transition metal-catalyzed oxidation of atmospheric sulfur: Global implications for the sulfur budget, J. Geophys. Res.-Atmos., 114, https://doi.org/10.1029/2008JD010486, 2009.
- Baker, A. R. and Jickells, T. D.: Mineral particle size as a control on aerosol iron solubility, Geophys. Res. Lett., 33, https://doi.org/10.1029/2006GL026557, 2006.
- 810 Bi, X., Dai, Q., Wu, J., Zhang, Q., Zhang, W., Luo, R., Cheng, Y., Zhang, J., Wang, L., Yu, Z., Zhang, Y., Tian, Y., and Feng, Y.: Characteristics of the main primary source profiles of particulate matter across China from 1987 to 2017, Atmos. Chem. Phys., 19, 3223–3243, https://doi.org/10.5194/acp-19-3223-2019, 2019.
 - Binkowski, F. S. and Roselle, S. J.: Models-3 community multiscale air quality (CMAQ) model aerosol component 1. Model description, J. Geophys. Res.-Atmos., 108, https://doi.org/10.1029/2001JD001409, 2003.
- Bunnell, Z. B., Sieber, M., Hamilton, D. S., Marsay, C. M., Buck, C. S., Landing, W. M., John, S. G., and Conway, T. M.: The influence of natural, anthropogenic, and wildfire sources on iron and zinc aerosols delivered to the North Pacific Ocean, Geophys. Res. Lett., 52, https://doi.org/10.1029/2024GL113877, 2025.



860



- Cao, J.: PM_{2.5} and the environment in China, Science Press, Beijing, China, ISBN 9787030403827, 2014.
- Chen, D., Wang, X., Li, Y., Lang, J., Zhou, Y., Guo, X., and Zhao, Y.: High-spatiotemporal-resolution ship emission inventory of China based on AIS data in 2014, Sci. Total Environ., 609, 776–787, https://doi.org/10.1016/j.scitotenv.2017.07.051, 2017.
 - Chen, Y., Wang, Z., Fang, Z., Huang, C., Xu, H., Zhang, H., Zhang, T., Wang, F., Luo, L., Shi, G., Wang, X., and Tang, M.: Dominant contribution of non-dust primary emissions and secondary processes to dissolved aerosol iron, Environ. Sci. Technol., 58, 17355-17363, https://doi.org/10.1021/acs.est.4c05816, 2024.
- China Meteorological Administration (CMA): Meteorological bulletin of atmospheric environment, 2021. Available at: https://www.cma.gov.cn/zfxxgk/gknr/qxbg/202301/t20230119 5273410.html (last accessed: September 22, 2025).
 - China Meteorological Administration (CMA): Meteorological bulletin of atmospheric environment, 2022. Available at: https://www.cma.gov.cn/zfxxgk/gknr/qxbg/202307/t20230707 5633816.html (last accessed: September 22, 2025).
- Conway, T. M., Hamilton, D. S., Shelley, R. U., Aguilar-Islas, A. M., Landing, W. M., Mahowald, N. M., and John, S. G.: Tracing and constraining anthropogenic aerosol iron fluxes to the North Atlantic Ocean using iron isotopes, Nat. Commun., 10, https://doi.org/10.1038/s41467-019-10457-w, 2019.
 - Desboeufs, K. V., Losno, R., and Colin, J. L.: Factors influencing aerosol solubility during cloud processes, Atmos. Environ., 35, 3529–3537, https://doi.org/10.1016/S1352-2310(00)00472-6, 2001.
- Dong, X., Zhang, Y., Yu, G., Xiong, Y., Han, Z., Huo, J., Huang, C., Kan, H., Zheng, M., Ning, Z., and Xie, B.: Environmental and health impacts of reduced PM_{2.5} and trace metals from ship emissions under low-sulfur fuel oil policy in Shanghai, China, Environ. Pollut., 377, https://doi.org/10.1016/j.envpol.2025.126409, 2025.
 - Fu, H., Lin, J., Shang, G., Dong, W., Grassian, V. H., Carmichael, G. R., Li, Y., and Chen, J.: Solubility of iron from combustion source particles in acidic media linked to iron speciation, Environ. Sci. Technol., 46, 11119–11127, https://doi.org/10.1021/es302558m, 2012.
- 640 Gao, Y., Xu, G., Zhan, J., Zhang, J., Li, W., Lin, Q., Chen, L., and Lin, H.: Spatial and particle size distributions of atmospheric dissolvable iron in aerosols and its input to the Southern Ocean and coastal East Antarctica, J. Geophys. Res.-Atmos., 118, 12634–12648, https://doi.org/10.1002/2013JD020367, 2013.
- Gary, N., Rachelle, D., Steve, B., and Song, B.: EPA positive matrix factorization (PMF) 5.0 fundamentals and user guide, U.S. Environmental Protection Agency, Washington, USA, 2014. Available at: https://www.epa.gov/sites/default/files/2015-02/documents/pmf_5.0_user_guide.pdf (last accessed: September 22, 2025).
 - Ge, Y., Guan, W., Wong, K. H., and Zhang, R.: Spatial variability and source identification of trace elements in aerosols from Northwest Pacific Marginal Sea, Indian Ocean and South Pacific to Antarctica, Glob. Biogeochem. Cycle, 38, https://doi.org/10.1029/2024GB008235, 2024.
- 850 Gledhill, M. and Buck, K. N.: The organic complexation of iron in the marine environment: a review, Front. Microbiol., 3, https://doi.org/10.3389/fmicb.2012.00069, 2012.
 - Guo, L., Chen, Y., Wang, F., Meng, X., Xu, Z., and Zhuang, G.: Effects of Asian dust on the atmospheric input of trace elements to the East China Sea, Mar. Chem., 163, 19–27, https://doi.org/10.1016/j.marchem.2014.04.003, 2014.
- Hamilton, D. S., Scanza, R. A., Rathod, S. D., Bond, T. C., Kok, J. F., Li, L., Matsui, H., and Mahowald, N. M.: Recent (1980 to 2015) trends and variability in daily-to-interannual soluble iron deposition from dust, fire, and anthropogenic sources, Geophys. Res. Lett., 47, https://doi.org/10.1029/2020GL089688, 2020.
 - Hamilton, D. S., Scanza, R. A., Feng, Y., Guinness, J., Kok, J. F., Li, L., Liu, X., Rathod, S. D., Wan, J. S., Wu, M., and Mahowald, N. M.: Improved methodologies for Earth system modelling of atmospheric soluble iron and observation comparisons using the Mechanism of Intermediate complexity for Modelling Iron (MIMI v1.0), Geosci. Model Dev., 12, 3835–3862, https://doi.org/10.5194/gmd-12-3835-2019, 2019.
 - Hsu, S. C., Wong, G. T. F., Gong, G. C., Shiah, F. K., Huang, Y. T., Kao, S. J., Tsai, F., Lung, S. C. C., Lin, F. J., Lin, I. I., Hung, C. C., and Tseng, C. M.: Sources, solubility, and dry deposition of aerosol trace elements over the East China Sea, Mar. Chem., 120, 116–127, https://doi.org/10.1016/j.marchem.2008.10.003, 2010.
 - Huang, S. L., Rahn, K. A., Arimoto, R.: Testing and optimizing two factor-analysis techniques on aerosol at Narragansett, Rhode Island, Atmos. Environ., 33, 2169–2185, https://doi.org/10.1016/S1352-2310(98)00324-0, 1999.
 - Ito, A.: Global modeling study of potentially bioavailable iron input from shipboard aerosol sources to the ocean, Glob. Biogeochem. Cycle, 27, 1–10, https://doi.org/10.1029/2012GB004378, 2013.



880



- Ito, A.: Atmospheric processing of combustion aerosols as a source of bioavailable iron, Environ. Sci. Technol. Lett., 2, 70–75, https://doi.org/10.1021/acs.estlett.5b00007, 2015.
- 870 Ito, A. and Miyakawa, T.: Aerosol iron from metal production as a secondary source of bioaccessible iron, Environ. Sci. Technol., 57, 4091–4100, https://doi.org/10.1021/acs.est.2c06472, 2023.
 - Ito, A., Ye, Y., Baldo, C., and Shi, Z.: Ocean fertilization by pyrogenic aerosol iron, npj Clim. Atmos. Sci., 4, https://doi.org/10.1038/s41612-021-00185-8, 2021.
- Ito, A., Myriokefalitakis, S., Kanakidou, M., Mahowald, N. M., Scanza, R. A., Hamilton, D. S., Baker, A. R., Jickells, T., Sarin, M., Bikkina, S., Gao, Y., Shelley, R. U., Buck, C. S., Landing, W. M., Bowie, A. R., Perron, M. M. G., Guieu, C., Meskhidze, N., Johnson, M. S., Feng, Y., Kok, J. F., Nenes, A., and Duce, R. A.: Pyrogenic iron: The missing link to high iron solubility in aerosols, Sci. Adv., 5, https://doi.org/10.1126/sciadv.aau7671, 2019.
 - Ji, D., Liu, Y., Xu, X., He, J., Liu, N., Ge, B., and Wang, Y.: Abundance, distribution and deposition of PM_{2.5}-bound iron in northern China during 2021 dust and dust storm periods, Atmos. Environ., 318, https://doi.org/10.1016/j.atmosenv.2023.120249, 2024.
 - Jiang, S., Zhang, Y., Yu, G., Han, Z., Zhao, J., Zhang, T., and Zheng, M.: Source-resolved atmospheric metal emissions, concentrations, and deposition fluxes into the East Asian seas, Atmos. Chem. Phys., 24, 8363–8381, https://doi.org/10.5194/acp-24-8363-2024, 2024.
- Jickells, T. D., An, Z. S., Andersen, K. K., Baker, A. R., Bergametti, G., Brooks, N., Cao, J., Boyd, P. W., Duce, R. A., Hunter, K. A., Kawahata, H., Kubilay, N., laRoche, J., Liss, P. S., Mahowald, N., Prospero, J. M., Ridgwell, A. J., Tegen, I., and Torres, R.: Global iron connections between desert dust, ocean biogeochemistry, and climate, Science, 308, 67–71, https://doi.org/10.1126/science.1105959, 2005.
 - Johansson, L., Jalkanen, J. P., and Kukkonen, J.: Global assessment of shipping emissions in 2015 on a high spatial and temporal resolution, Atmos. Environ., 167, 403–415, https://doi.org/10.1016/j.atmosenv.2017.08.042, 2017.
- Johnson, M. S. and Meskhidze, N.: Atmospheric dissolved iron deposition to the global oceans: effects of oxalate-promoted Fe dissolution, photochemical redox cycling, and dust mineralogy, Geosci. Model Dev., 6, 1137–1155, https://doi.org/10.5194/gmd-6-1137-2013, 2013.
 - König, D., Conway, T. M., Hamilton, D. S., and Tagliabue, A.: Surface ocean biogeochemistry regulates the impact of anthropogenic aerosol Fe deposition on the cycling of iron and iron isotopes in the North Pacific, Geophys. Res. Lett., 49, https://doi.org/10.1029/2022GL098016, 2022.
 - Krishnamurthy, A., Moore, J. K., Mahowald, N., Luo, C., Doney, S. C., Lindsay, K., and Zender, C. S.: Impacts of increasing anthropogenic soluble iron and nitrogen deposition on ocean biogeochemistry, Glob. Biogeochem. Cycle, 23, https://doi.org/10.1029/2008GB003440, 2009.
- Kurisu, M., Sakata, K., Uematsu, M., Ito, A., and Takahashi, Y.: Contribution of combustion Fe in marine aerosols over the northwestern Pacific estimated by Fe stable isotope ratios, Atmos. Chem. Phys., 21, 16027–16050, https://doi.org/10.5194/acp-21-16027-2021, 2021.
 - Lambert, F., Tagliabue, A., Shaffer, G., Lamy, F., Winckler, G., Farias, L., Gallardo, L., and De Pol-Holz, R.: Dust fluxes and iron fertilization in Holocene and Last Glacial Maximum climates, Geophys. Res. Lett., 42, 6014–6023, https://doi.org/10.1002/2015GL064250, 2015.
- 905 Lee, S., Han, C., Shin, D., Hur, S. D., Jun, S. J., Kim, Y. T., Byun, D. S., and Hong, S.: Characteristics of elemental and Pb isotopic compositions in aerosols (PM_{10-2.5}) at the Ieodo Ocean Research Station in the East China Sea, Environ. Pollut., 231, 154–164, https://doi.org/10.1016/j.envpol.2017.08.007, 2017.
 - Li, T. and Yuan, H.: Element abundance in the oceanic and the continental lithospheres, Geochimica, 40, 1–5, https://doi.org/10.19700/j.0379-1726.2011.01.001, 2011.
- 910 Lin, Y. C., Chen, J. P., Ho, T. Y., and Tsai, I. C.: Atmospheric iron deposition in the northwestern Pacific Ocean and its adjacent marginal seas: The importance of coal burning, Glob. Biogeochem. Cycle, 29, 138–159, https://doi.org/10.1002/2013GB004795, 2015.
- Liu, J., Zhang, T., Ding, X., Li, X., Liu, Y., Yan, C., Shen, Y., Yao, X., and Zheng, M.: A clear north-to-south spatial gradience of chloride in marine aerosol in Chinese seas under the influence of East Asian Winter Monsoon, Sci. Total Environ., 832, https://doi.org/10.1016/j.scitotenv.2022.154929, 2022a.



920

925



- Liu, M., Matsui, H., Hamilton, D. S., Lamb, K. D., Rathod, S. D., Schwarz, J. P., and Mahowald, N. M.: The underappreciated role of anthropogenic sources in atmospheric soluble iron flux to the Southern Ocean, npj Clim. Atmos. Sci., 5, https://doi.org/10.1038/s41612-022-00250-w, 2022b.
- Liu, Y., Xing, J., Wang, S., Fu, X., and Zheng, H.: Source-specific speciation profiles of PM_{2.5} for heavy metals and their anthropogenic emissions in China, Environ. Pollut., 239, 544–553, https://doi.org/10.1016/j.envpol.2018.04.047, 2018.
- Mahowald, N. M., Hamilton, D. S., Mackey, K. R. M., Moore, J. K., Baker, A. R., Scanza, R. A., and Zhang, Y.: Aerosol trace metal leaching and impacts on marine microorganisms, Nat. Commun., 9, https://doi.org/10.1038/s41467-018-04970-7, 2018.
- Martin, J. H.: Glacial-interglacial CO₂ change: The iron hypothesis, Paleoceanography, 5, 1–13, https://doi.org/10.1029/PA005i001p00001, 1990.
- Matsui, H., Mahowald, N. M., Moteki, N., Hamilton, D. S., Ohata, S., Yoshida, A., Koike, M., Scanza, R. A., and Flanner, M. G.: Anthropogenic combustion iron as a complex climate forcer, Nat. Commun., 9, https://doi.org/10.1038/s41467-018-03997-0, 2018.
- Meng, L., Yang, X., Zhao, T., He, Q., Lu, H., Mamtimin, A., Huo, W., Yang, F., and Liu, C.: Modeling study on three-dimensional distribution of dust aerosols during a dust storm over the Tarim Basin, Northwest China, Atmos. Res., 218, 285–295, https://doi.org/10.1016/j.atmosres.2018.12.006, 2019.
 - Meng, Q., Yan, C., Li, R., Zhang, T., Zheng, M., Liu, Y., Zhang, M., Wang, G., Du, Y., Shang, C., and Fu, P.: Variations of PM_{2.5}-bound elements and their associated effects during long-distance transport of dust storms: Insights from multisites observations, Sci. Total Environ., 889, https://doi.org/10.1016/j.scitotenv.2023.164062, 2023.
- Myriokefalitakis, S., Ito, A., Kanakidou, M., Nenes, A., Krol, M. C., Mahowald, N. M., Scanza, R. A., Hamilton, D. S., Johnson, M. S., Meskhidze, N., Kok, J. F., Guieu, C., Baker, A. R., Jickells, T. D., Sarin, M. M., Bikkina, S., Shelley, R., Bowie, A., Perron, M. M. G., and Duce, R. A.: Reviews and syntheses: the GESAMP atmospheric iron deposition model intercomparison study, Biogeosciences, 15, 6659–6684, https://doi.org/10.5194/bg-15-6659-2018, 2018.
- Oakes, M., Ingall, E. D., Lai, B., Shafer, M. M., Hays, M. D., Liu, Z. G., Russell, A. G., and Weber, R. J.: Iron solubility related to particle sulfur content in source emission and ambient fine particles, Environ. Sci. Technol., 46, 6637–6644, https://doi.org/10.1021/es300701c, 2012.
 - Paatero, P. and Tapper, U.: Positive matrix factorization: A nonnegative factor model with optimal utilization of error estimates of data values, Environmetrics, 5, 111–126, https://doi.org/10.1002/env.3170050203, 1994.
- Perron, M. M. G., Strzelec, M., Gault-Ringold, M., Proemse, B. C., Boyd, P. W., and Bowie, A. R.: Assessment of leaching protocols to determine the solubility of trace metals in aerosols, Talanta, 208, https://doi.org/10.1016/j.talanta.2019.120377, 2020.
 - Pinedo-González, P., Hawco, N. J., Bundy, R. M., Armbrust, E. V., Follows, M. J., Cael, B. B., White, A. E., Ferrón, S., Karl, D. M., and John, S. G.: Anthropogenic Asian aerosols provide Fe to the North Pacific Ocean, Proc. Natl. Acad. Sci. U. S. A., 117, 27862–27868, https://doi.org/10.1073/pnas.2010315117, 2020.
- Rathod, S. D., Hamilton, D. S., Mahowald, N. M., Klimont, Z., Corbett, J. J., and Bond, T. C.: A mineralogy-based anthropogenic combustion-iron emission inventory, J. Geophys. Res.-Atmos., 125, https://doi.org/10.1029/2019JD032114, 2020.
 - Scanza, R. A., Hamilton, D. S., Perez Garcia-Pando, C., Buck, C., Baker, A., and Mahowald, N. M.: Atmospheric processing of iron in mineral and combustion aerosols: development of an intermediate-complexity mechanism suitable for Earth system models, Atmos. Chem. Phys., 18, 14175–14196, https://doi.org/10.5194/acp-18-14175-2018, 2018.
 - Scheirer, C. J., Ray, W. S., and Hare, N.: The analysis of ranked data derived from completely randomized factorial designs, Biometrics, 32, 429–434, https://doi.org/10.2307/2529511, 1976.
 - Schroth, A. W., Crusius, J., Sholkovitz, E. R., and Bostick, B. C.: Iron solubility driven by speciation in dust sources to the ocean, Nat. Geosci., 2, 337–340, https://doi.org/10.1038/NGEO501, 2009.
- 960 Seo, H. and Kim, G.: Anthropogenic iron invasion into the ocean: results from the East Sea (Japan Sea), Environ. Sci. Technol., 57, 10745–10753, https://doi.org/10.1021/acs.est.3c01084, 2023.
 - Shi, J., Guan, Y., Ito, A., Gao, H., Yao, X., Baker, A. R., and Zhang, D.: High production of soluble iron promoted by aerosol acidification in fog, Geophys. Res. Lett., 47, https://doi.org/10.1029/2019GL086124, 2020.



980

985

995

1000



- Sholkovitz, E. R., Sedwick, P. N., Church, T. M., Baker, A. R., and Powell, C. F.: Fractional solubility of aerosol iron:

 Synthesis of a global-scale data set, Geochim. Cosmochim. Acta, 89, 173–189,
 https://doi.org/10.1016/j.gca.2012.04.022, 2012.
 - Tagliabue, A., Bowie, A. R., Boyd, P. W., Buck, K. N., Johnson, K. S., and Saito, M. A.: The integral role of iron in ocean biogeochemistry, Nature, 543, 51–59, https://doi.org/10.1038/nature21058, 2017.
- Tai, A. P. K., Ma, P. H. L., Chan, Y. C., Chow, M. K., Ridley, D. A., and Kok, J. F.: Impacts of climate and land cover variability and trends on springtime East Asian dust emission over 1982–2010: A modeling study, Atmos. Environ., 254, https://doi.org/10.1016/j.atmosenv.2021.118348, 2021.
 - Takahashi, Y., Higashi, M., Furukawa, T., and Mitsunobu, S.: Change of iron species and iron solubility in Asian dust during the long-range transport from western China to Japan, Atmos. Chem. Phys., 11, 11237–11252, https://doi.org/10.5194/acp-11-11237-2011, 2011.
- 975 Tang, Y., Jia, X., Huang, C., Wang, F., Ren, Y., Gu, W., Li, R., Zhang, G., and Tang, M.: Dissolution characteristics of typical iron-containing minerals, J. Earth Environ., 14, 136–144, https://doi.org/10.7515/JEE222007, 2023.
 - Tian, H., Zhu, C., Gao, J., Cheng, K., Hao, J., Wang, K., Hua, S., Wang, Y., and Zhou, J.: Quantitative assessment of atmospheric emissions of toxic heavy metals from anthropogenic sources in China: historical trend, spatial distribution, uncertainties, and control policies, Atmos. Chem. Phys., 15, 10127–10147, https://doi.org/10.5194/acp-15-10127-2015, 2015.
 - Wang, L., Qi, J., Shi, J., Chen, X., and Gao, H.: Source apportionment of particulate pollutants in the atmosphere over the Northern Yellow Sea, Atmos. Environ., 70, 425–434, https://doi.org/10.1016/j.atmosenv.2012.12.041, 2013.
 - Wang, R., Balkanski, Y., Boucher, O., Bopp, L., Chappell, A., Ciais, P., Hauglustaine, D., Peñuelas, J., and Tao, S.: Sources, transport and deposition of iron in the global atmosphere, Atmos. Chem. Phys., 15, 6247–6270, https://doi.org/10.5194/acp-15-6247-2015, 2015.
 - Xu, L., Zhi, M., Liu, X., Gao, H., Yao, X., Yuan, Q., Fu, P., and Li, W.: Direct evidence of pyrogenic aerosol iron by intrusions of continental polluted air into the Eastern China Seas, Atmos. Res., 292, https://doi.org/10.1016/j.atmosres.2023.106839, 2023.
- Yanca, C. A., Barth, D. C., Petterson, K. A., Nakanishi, M. P., Cooper, J. A., Johnsen, B. E., Lambert, R. H., and Bivins, D.
 G.: Validation of three new methods for determination of metal emissions using a modified environmental protection agency method 301, J. Air Waste Manage. Assoc., 56, 1733–1742, https://doi.org/10.1080/10473289.2006.10464578, 2006.
 - Yang, T., Chen, Y., Zhou, S., Li, H., Wang, F., and Zhu, Y.: Solubilities and deposition fluxes of atmospheric Fe and Cu over the Northwest Pacific and its marginal seas, Atmos. Environ., 239, https://doi.org/10.1016/j.atmosenv.2020.117763, 2020.
 - Yin, Z., Wan, Y., Zhang, Y., and Wang, H.: Why super sandstorm 2021 in North China?, Natl. Sci. Rev., 9, https://doi.org/10.1093/nsr/nwab165, 2022.
 - Li, Y., Liu, S., Luo, L., Yang, S., Lu, B., Wang, C., Hsu, S. C., and Kao, S.: Seasonal variations, source apportionment and dry deposition of chemical species of total suspended particulate in Pengjia Yu Island, East China Sea, Mar. Pollut. Bull., 187, https://doi.org/10.1016/j.marpolbul.2023.114608, 2023.
 - Yu, G., Zhang, Y., Yang, F., He, B., Zhang, C., Zou, Z., Yang, X., Li, N., and Chen, J.: Dynamic Ni/V ratio in the ship-emitted particles driven by multiphase fuel oil regulations in coastal China, Environ. Sci. Technol., 55, 15031–15039, https://doi.org/10.1021/acs.est.1c02612, 2021.
- Yu, H., Yang, Y., Wang, H., Tan, Q., Chin, M., Levy, R. C., Remer, L. A., Smith, S. J., Yuan, T., and Shi, Y.: Interannual variability and trends of combustion aerosol and dust in major continental outflows revealed by MODIS retrievals and CAM5 simulations during 2003-2017, Atmos. Chem. Phys., 20, 139–161, https://doi.org/10.5194/acp-20-139-2020, 2020.
 - Zhang, F., Chen, Y., Wang, X., Tian, C., Tang, J., Li, J., and Zhang, G.: Chemical compositions and seasonal variation of PM_{2.5} in the National Air Background Monitoring Station at Tuoji Island, Geochimica, 43, 317–328, https://doi.org/10.19700/j.0379-1726.2014.04.001, 2014a.
 - Zhang, F., Chen, Y., Chen, Q., Feng, Y., Shang, Y., Yang, X., Gao, H., Tian, C., Li, J., Zhang, G., Matthias, V., and Xie, Z.: Real-world emission factors of gaseous and particulate pollutants from marine fishing boats and their total emissions in China, Environ. Sci. Technol., 52, 4910–4919, https://doi.org/10.1021/acs.est.7b04002, 2018.



1020

1025

1030



- Zhang, H., Li, R., Dong, S., Wang, F., Zhu, Y., Meng, H., Huang, C., Ren, Y., Wang, X., Hu, X., Li, T., Peng, C., Zhang, G., Xue, L., Wang, X., and Tang, M.: Abundance and fractional solubility of aerosol iron during winter at a coastal city in Northern China: Similarities and contrasts between fine and coarse particles, J. Geophys. Res.-Atmos., 127, https://doi.org/10.1029/2021JD036070, 2022.
 - Zhang, J., Liu, X., Wang, J., He, H., Yao, X., and Gao, H.: Atmospheric dry deposition fluxes of trace metals over the Eastern China Marginal Seas: Impact of emission controls, Sci. Total Environ., 873, https://doi.org/10.1016/j.scitotenv.2023.162117, 2023a.
 - Zhang, K. and Gao, H.: The characteristics of Asian-dust storms during 2000–2002: From the source to the sea, Atmos. Environ., 41, 9136–9145, https://doi.org/10.1016/j.atmosenv.2007.08.007, 2007.
 - Zhang, Q., Zheng, Y., Tong, D., Shao, M., Wang, S., Zhang, Y., Xu, X., Wang, J., He, H., Liu, W., Ding, Y., Lei, Y., Li, J., Wang, Z., Zhang, X., Wang, Y., Cheng, J., Liu, Y., Shi, Q., Yan, L., Geng, G., Hong, C., Li, M., Liu, F., Zheng, B., Cao, J., Ding, A., Gao, J., Fu, Q., Huo, J., Liu, B., Liu, Z., Yang, F., He, K., and Hao, J.: Drivers of improved PM_{2.5} air quality in China from 2013 to 2017, Proc. Natl. Acad. Sci. U. S. A., 116, 24463–24469, https://doi.org/10.1073/pnas.1907956116, 2019.
 - Zhang, R., Cao, J., Tang, Y., Arimoto, R., Shen, Z., Wu, F., Han, Y., Wang, G., Zhang, J., and Li, G.: Elemental profiles and signatures of fugitive dusts from Chinese deserts, Sci. Total Environ., 472, 1121–1129, https://doi.org/10.1016/j.scitotenv.2013.11.011, 2014b.
 - Zhang, T. and Zheng, M.: Atmospheric iron in Chinese marginal seas and the Northwest Pacific: A review, China Environ. Sci., 44, 602–619, https://doi.org/10.19674/j.cnki.issn1000-6923.2024.0046, 2024.
 - Zhang, T., Liu, J., Xiang, Y., Liu, X., Zhang, J., Zhang, L., Ying, Q., Wang, Y., Wang, Y., Chen, S., Chai, F., and Zheng, M.: Quantifying anthropogenic emission of iron in marine aerosol in the Northwest Pacific with shipborne online measurements, Sci. Total Environ., 912, https://doi.org/10.1016/j.scitotenv.2023.169158, 2024.
 - Zhang, T., Zheng, M., Sun, X., Chen, H., Wang, Y., Fan, X., Pan, Y., Quan, J., Liu, J., Wang, Y., Lyu, D., Chen, S., Zhu, T., and Chai, F.: Environmental impacts of three Asian dust events in the northern China and the northwestern Pacific in spring 2021, Sci. Total Environ., 859, https://doi.org/10.1016/j.scitotenv.2022.160230, 2023b.
- Zhang, Y., Yang, X., Brown, R., Yang, L., Morawska, L., Ristovski, Z., Fu, Q., and Huang, C.: Shipping emissions and their impacts on air quality in China, Sci. Total Environ., 581–582, 186–198, https://doi.org/10.1016/j.scitotenv.2016.12.098, 2017.
 - Zhao, M., Zhang, Y., Ma, W., Fu, Q., Yang, X., Li, C., Zhou, B., Yu, Q., and Chen, L.: Characteristics and ship traffic source identification of air pollutants in China's largest port, Atmos. Environ., 64, 277–286, https://doi.org/10.1016/j.atmosenv.2012.10.007, 2013.
- Zhu, H., Liu, Y., Yue, M., Feng, S., Fu, P., Huang, K., Dong, X., and Wang, M.: Trends and drivers of soluble iron deposition from East Asian dust to the Northwest Pacific: a springtime analysis (2001–2017), Atmos. Chem. Phys., 25, 5175–5197, https://doi.org/10.5194/acp-25-5175-2025, 2025.
- Zhu, Y., Li, W., Wang, Y., Zhang, J., Liu, L., Xu, L., Xu, J., Shi, J., Shao, L., Fu, P., Zhang, D., and Shi, Z.: Sources and processes of iron aerosols in a megacity in Eastern China, Atmos. Chem. Phys., 22, 2191–2202, https://doi.org/10.5194/acp-22-2191-2022, 2022.